10/4-24-91 JSD

SANDIA REPORT

SAND90—0252
Unlimited Release
Printed February 1991

Yucca Mountain Site Characterization Project

The Distribution of Moisture Beneath a Two-Dimensional Surface Source

M. J. Martinez, D. F. McTigue

Prepared by
Sandia National Laboratories
Albuquerque, New Mexico 87185 and Livermore, California 94550
for the United States Department of Energy
under Contract DE-AC04-76DP00789

"Prepared by Yucca Mountain Site Characterization Project (YMSCP) participants as part of the Civilian Radioactive Waste Management Program (CRWM). The YMSCP is managed by the Yucca Mountain Project Office of the U.S. Department of Energy, Nevada Operations Office (DOE/NV). YMSCP work is sponsored by the Office of Geologic Repositories (OGR) of the DOE Office of Civilian Radioactive Waste Management (OCRWM)."

Issued by Sandia National Laboratories, operated for the United States Department of Energy by Sandia Corporation.

Available to DOE and DOE contractors from
Office of Scientific and Technical Information
PO Box 62
Oak Ridge, TN 37831

Prices available from (615) 576-8401, FTS 626-8401

Available to the public from
National Technical Information Service
US Department of Commerce
5285 Port Royal Rd
Springfield, VA 22161

NTIS price codes
Printed copy: A04
Microfiche copy: A01

SAND--90-0252

DE91 010720

SAND90-0252
Unlimited Release
Printed March 1991

The Distribution of Moisture Beneath a Two-Dimensional Surface Source

M. J. Martinez
D. F. McTigue
Fluid, Thermal and Structural Sciences Department
Sandia National Laboratories
Albuquerque, New Mexico 87185

Abstract

The distribution of moisture beneath a two-dimensional strip source is analyzed by applying the quasi-linear approximation. The source is described by specifying either the moisture content or the infiltration rate. A water table is specified at some depth, D, below the surface, the depth varying from shallow to semi-infinite. Numerical solutions are determined, via the boundary integral equation method, as a function of material sorptivity, α, the width of the strip source, $2L$, and the depth to the water table. The moisture introduced at the source is broadly spread below the surface when $\alpha L \ll 1$, for which absorption by capillary forces is dominant over gravity-induced flow. Conversely, the distribution becomes finger-like along the vertical when $\alpha L \gg 1$, where gravity is dominant over absorption. For a source described by specifying the moisture content, the presence of a water table at finite depth influences the infiltration through the source when αD is less than about 4; infiltration rates obtained when the water table depth is semi-infinite are of sufficient accuracy for greater values of αD. When the source is described by a specified infiltration flux, the maximum allowable value of this flux for which the material beneath the source remains unsaturated is determined as a function of nondimensional sorptivity and depth to the water table.

The work contained in this report was done at Quality Assurance Level NQ and pertains to WBS Element 1.2.1.4.4.1.

Contents

Tables

Figures

1 Introduction

In this paper we consider the steady infiltration of moisture from a strip surface source of width $2L$ into a homogeneous, porous half-plane. The porous layer is unsaturated for some depth D below the surface, where a horizontal water table exists. The hydraulic conductivity, K, of the porous material is assumed to vary with pressure head according to

$$K(\psi) = K_s \exp(\alpha\psi) \,, \quad \psi \leq 0, \tag{1.1}$$

where K_s is the saturated conductivity, α is a material parameter, and ψ is capillary pressure head. With this specification for hydraulic conductivity, the Kirchhoff transformation renders a linear field equation for a potential, which is equivalent to the relative permeability. This approach is referred to as a quasi-linear analysis after Philip (1968), who has vigorously pursued this approximation (see for example Philip, 1969; Philip, 1984a; Philip, 1989a; Philip, et al., 1989a; Philip, et al., 1989b; Waechter and Philip, 1985; and references therein).

Our purpose here is to investigate the steady distribution of moisture beneath a strip source as a function of the material sorptivity, α, a term coined by Waechter and Philip (1985), and the depth to the water table, D. Localized surface sources arise due to topographic relief or from shallow ponds (Weir, 1986; Wooding, 1968). The problem is prototypical of steady surface infiltration and the subsurface redistribution of the moisture as a function of the type of porous material. The problem is also relevant to the distribution of surface moisture introduced for irrigation (e.g., drip systems) or for dust control, and will describe the maximum wetting possible because the source is constant in time.

1.1 Previous Work

A rather complete review of infiltration from surface sources is given by Pullan (1990), however for completeness we review some of the more relevant works here. The axisymmetric version of the problem, when the moisture is specified at the source and the water table is deep, was considered by Wooding (1968), however, his solution method failed to converge for large values of αL. More recently, Weir (1986) considered the region local to the step change in boundary condition type, viz., the region about $|X| = L$, and derived an expression, deduced earlier by Wooding, for the net infiltration when αL is large. Pullan and Collins (1987) applied a boundary integral method to various problems of two- and three-dimensional infiltration from buried and surface cavities, also assuming a deep water table. Pullan and Collins computed the net flux through the source area of a two-dimensional source for a specified-moisture boundary condition; however, no discussion of the distribution of moisture beneath the surface was offered. Philip (1989b) recently considered the effect of a water table at finite depth below a buried source and finds the deep water table solutions to apply if the depth is greater than about $8/\alpha$.

Steady infiltration from a periodic array of line sources was considered by Raats (1970), and subsequently Batu (1978) considered steady infiltration from single and periodic strip sources. Batu's solution for the single strip source is rather formal, given in terms of a Fourier integral, and numerical evaluation is performed only for $\alpha L = 0.2$ and 0.5. These investigations are also based on the quasilinear assumption and the sources are described by specifying the strength of the line source (Raats, 1970; Zachmann, 1978), or the infiltration rate on the strip, (Batu, 1978). These specified infiltration problems can also be formulated in terms of a stream function, as shown by Raats (1970). Batu (1980), and Batu and Gardner (1978) also present solutions for periodic strip sources with nonuniform infiltration formulated in terms of a stream function. However, Philip (1984b), points out the danger of specifying the problem solely in kinematic terms, which can lead to physically untenable solutions if the flow dynamics are not considered in tandem. Zachmann (1978) considered infiltration from a line source into an inclined porous layer and presents series solutions for moisture potential and a stream function.

Here, we apply a boundary integral equation method to the quasi-linear version of the problem, as do Pullan and Collins (1987) for the case of a deep water table; we consider the effects of a shallow water table as well. Moreover, we also discuss the problem where the source is described by specifying the infiltration flux rather than the moisture and determine the maximum infiltration allowable such that the underlying material remains unsaturated. This latter bound on the allowable infiltration is not discussed in the study by Batu (1978) of this problem for a deep water table. Our discussion of this problem also includes the effects of a shallow water table.

Finally, we point out that our work with the boundary integral equation method, although similar to Pullan and Collins (1987), is formulated in a slightly different manner; they work with a transformed equation utilizing a transformation apparently due to Oseen (see Lamb, 1945; p. 611). These differences are minor; the major point is the ease with which numerical solutions of the quasilinear equation for steady, unsaturated flow can be obtained, over a large range of α, via the boundary integral equation method. Solutions for large values of a nondimensional α, to be introduced shortly, have been a source of difficulty in the summing of series solutions. Asymptotic treatment of this problem has been studied by Waechter and Philip (1985) who recognized the analogy with scattering of plane pulses and harmonic waves in hydrodynamics; a recent review is given by Philip (1989a). We also demonstrate that interior values of potential and flux can be computed using this method. Indeed, the method provides solutions for the flux vector that are of the same order of approximation as the potential itself. More conventional numerical methods, such as finite-difference or finite-element, in general provide a lower-order approximation for fluxes, since they involve finite-difference approximations to the potential gradient. We do point out, however, that the boundary integral equation method is restricted to problems governed by linear partial differential equations, although boundary conditions may be nonlinear, and that methods which preserve the accuracy for the fluxes obtained by finite-element techniques have been investigated

(Carey, 1982; Yeh, 1981).

2 Problem Statement

Two problems will be considered; both involve infiltration from a wetted source of width $2L$ into a relatively dry, homogeneous, porous material. The problems are distinguished by the depth to a water table below the source. The first problem considers the simpler case of a deep water table, in which the only parameter in the problem is a nondimensional sorptivity. In the second problem, the water table is located at finite depth below the surface and two more parameters arise, involving the depth and the specified moisture level (or flux) on the surface.

The flow is described by the steady Richards equation,

$$\nabla \cdot [K(\psi)(\nabla\psi - \mathbf{e}_z)] = 0, \tag{2.1}$$

where $\mathbf{e}_z$ is the unit vector in the vertical direction (positive downward). The boundary condition on the wetted strip is

$$\psi = \psi_o, \quad |X| < L, \ Z = 0, \tag{2.2}$$

and, assuming evaporation is negligible, zero vertical flux is prescribed over the remaining surface area (Wooding, 1968),

$$q_z = -K(\psi)\left(\frac{\partial\psi}{\partial Z} - 1\right) = 0, \quad |X| > L, \ Z = 0. \tag{2.3}$$

The related problem, where the source is described by specifying an infiltration flux rather than the moisture potential, is described by replacing (2.2) with

$$q_z = q_o, \quad |X| < L, \ Z = 0. \tag{2.4}$$

A water table is assumed to be located at a depth D below the surface, which is described by specifying

$$\psi = \psi_w, \quad \text{for all } X, \ Z = D. \tag{2.5}$$

The pressure head at depth D is prescribed arbitrarily as ψ_w for purposes of generality in the problem statement; however, $\psi_w = 0$ will properly describe a water table. If the water table is 'deep'* beneath the surface, the capillary pressure far below the source, and yet above the water table, approaches a constant value,

$$\psi \to \psi_\infty, \ \text{ as } \ |\mathbf{X}| \to \infty, \tag{2.6}$$

where $\mathbf{X} = (X, Z)$ (two-dimensional flow). We further assume that $K(\psi_\infty)/K(\psi_o) \ll 1$, and hence the far-field condition (2.6) can also be stated as

$$q_z \to 0, \ \text{ as } \ |\mathbf{X}| \to \infty. \tag{2.7}$$

The two cases, defined by a deep and shallow water table, are discussed fully in the following.

*This terminology is clarified in Section 6 which treats a shallow water table

3 Quasi-Linear Analysis

As was shown previously (Philip, 1968; Raats, 1970; Wooding, 1968), the Richards equation can be transformed into a linear form when the conductivity varies exponentially with capillary pressure. By introducing the Kirchhoff transformation,

$$\Phi = \int_{-\infty}^{\psi} K(\acute{\psi}) d\acute{\psi}, \tag{3.1}$$

the steady Richards equation becomes

$$\nabla^2 \Phi - \alpha \frac{\partial \Phi}{\partial Z} = 0, \tag{3.2}$$

when the conductivity is exponential in the capillary pressure as defined in (1.1). Also,

$$\alpha \Phi = K(\psi), \quad \text{and} \quad \alpha \psi = \ln \phi, \tag{3.3}$$

where $\phi = K(\psi)/K_s = \exp(\alpha\psi) = \alpha\Phi/K_s$ is the relative permeability, which also satisfies (3.2). Furthermore, under the Kirchhoff transformation, the Darcy flux,

$$\mathbf{q} = -K(\psi)\nabla\psi + K(\psi)\mathbf{e}_z, \tag{3.4}$$

becomes

$$\mathbf{q} = -\nabla\Phi + \alpha\Phi\mathbf{e}_z, \tag{3.5}$$

so that the flux is also a linear function of the potential Φ (or ϕ). Essential and natural boundary conditions for the steady Richards equation also remain linear under the transformation for homogeneous materials. Owing to the relations given in (3.3), a contour level of constant potential is also a contour level of constant capillary pressure and moisture content (θ). This relation indicates that the potential Φ in (3.1) is uniquely related to the moisture content. It is noted that the retention curve for the material, specifying the function $\theta(\psi)$, is not required for solution of the steady Richards equation.

In terms of the transformed variables, the boundary conditions (2.2) and (2.6) become

$$\Phi = \alpha^{-1} K(\psi_o) = \Phi_o, \quad |X| < 1, \quad Z = 0, \tag{3.6}$$

and

$$\Phi = \alpha^{-1} K(\psi_\infty) = \Phi_\infty, \quad \mathbf{X} \to \infty, \tag{3.7}$$

respectively, and the impermeable condition (2.3) becomes

$$-\frac{\partial \Phi}{\partial Z} + \alpha\Phi = 0, \quad |X| > 1, \quad Z = 0. \tag{3.8}$$

Also, the shallow water table is specified by

$$\Phi = \alpha^{-1} K_s, \quad \text{for all } X, \; Z = D. \tag{3.9}$$

4 Numerical Solution by the Boundary Integral Equation Method

4.1 Boundary Integral Equation Formulation

A number of numerical methods are available for the solution of (3.2). Here we consider the boundary integral equation (BIE) method. The application of this method is suggested by the fact that fundamental solutions are known for (3.2) in both two and three dimensions, and by favorable previous experience with the method in various branches of mathematical physics, e.g. (Brebbia, 1978; Cruse, 1969; Ingham and Kelmanson, 1984; Jaswon and Symm, 1977; Liggett and Liu, 1982). Boundary integral methods reduce the dimension of the problem by one, which is an appealing feature in general, and is especially useful for semi-infinite problems and some interface problems (Liggett and Liu, 1982; Martinez and Udell, 1989). Thus, in the present study, the two-dimensional boundary value problem is reduced to a one-dimensional BIE defined on the boundary of the two-dimensional domain. Here we consider only two-dimensional problems, but emphasize that another attractive aspect of the approach is that its extension to three dimensions, while not easy, is straightforward (Pullan and Collins, 1987).

The boundary integral formulation can be motivated through Green's second identity,

$$\int_\Omega (G\nabla^2\Phi - \Phi\nabla^2 G)d\Omega = \int_\Gamma \left(G\frac{\partial\Phi}{\partial n} - \Phi\frac{\partial G}{\partial n} \right) d\Gamma. \tag{4.1}$$

Here, the volume Ω is bounded by the surface Γ, and, in the classical theory, Φ and G are nonsingular in Ω. Also, $\partial(\cdot)/\partial n = \nabla(\cdot)\cdot\mathbf{n}$, where $\mathbf{n}$ is the outward-pointing unit normal to the boundary. To generate the boundary integral, we use the free-space fundamental solution to (3.2) for G. The free-space Green's function satisfies

$$\nabla^2 G(\mathbf{x}) - \alpha\frac{\partial G}{\partial z} = -\delta(\mathbf{x}), \tag{4.2}$$

where z is the vertical coordinate (positive in the direction of gravity) and δ is the Dirac delta function. The two-dimensional solution can be found on p.267 of Carslaw and Jeager (1978) as the solution for a line source of unit strength placed at the origin:

$$G(\mathbf{x}) = \frac{1}{2\pi}\exp\left(\frac{\alpha z}{2}\right) K_0\left(\frac{\alpha r}{2}\right), \tag{4.3}$$

where $r^2 = x^2 + z^2$, and K_0 is the modified Bessel function of the second kind of order zero. The boundary integral equation results if we substitute the free-space Green's function (4.3), written with respect to the difference vector $\mathbf{x} - \mathbf{y}$, into (4.1), and integrate with respect to $\mathbf{y}$, to get

$$\Phi(\mathbf{x}) + \int_\Gamma \frac{\partial G(\mathbf{x},\mathbf{y})}{\partial n}\Phi(\mathbf{y})d\Gamma(\mathbf{y}) = \int_\Gamma G(\mathbf{x},\mathbf{y})(-q_n(\mathbf{y}))d\Gamma, \quad \mathbf{x}\in\Omega, \tag{4.4}$$

where $q_n(\mathbf{y}) = -\partial\Phi/\partial n + \alpha\Phi n_z$ is the flux normal to the boundary surface Γ, and $n_z = \mathbf{n}\cdot\mathbf{e}_z$ is the vertical component of the normal to Γ. This identity gives the value

of the potential at any point in Ω, if the boundary values of potential and flux are known. However, in a well-posed boundary value problem, either the potential or flux (or some combination of these) is specified and the other is to be determined. A boundary integral equation can be formulated for these unknowns by taking the limit $\mathbf{x} \rightarrow \Gamma$ from Ω; the limit is indicated because the flux kernel $\partial G/\partial n$ suffers a jump as $\mathbf{x}$ passes to the boundary from the interior. The resulting BIE, applied to a smooth point $\mathbf{x}$ on the boundary (i.e., one having a well-defined local tangent plane), is the same as (4.4) above if we multiply the first term on the left-hand side by one-half. Pullan and Collins (1987) show the values taken on by the principal value when $\mathbf{x}$ is on a corner of the boundary.

4.2 Numerical Solution

In this preliminary investigation of the quasi-linear method, the simplest of numerical approximations is used to facilitate coding of the algorithm. Higher order approximations (Martinez and Udell, 1989; Pullan and Collins, 1987) can be incorporated later if desired. The first step in the numerical approximation of (4.4) is to subdivide the boundary Γ into a number of discrete boundary elements, Γ_n ($n = 1, .., N$). In the present version, the boundary elements are all straight line segments. Next, the variation of Φ and q_n over each segment is approximated by its value at the center of the boundary element, hence the numerical approximation to the BIE becomes

$$\frac{1}{2}\Phi(\mathbf{x}_i) + \sum_j \Phi_j G'_{ij} = \sum_j (-q_{nj}) G_{ij}, \tag{4.5}$$

where $\Phi_j = \Phi(\mathbf{x}_j)$, $q_{nj} = q_n(\mathbf{x}_j)$, and

$$G'_{ij} = \int_{\Gamma_j} \frac{\partial G(\mathbf{x}_i, \mathbf{y})}{\partial n} d\Gamma(\mathbf{y}),$$

$$G_{ij} = \int_{\Gamma_j} G(\mathbf{x}_i, \mathbf{y}) d\Gamma(\mathbf{y}).$$

The coefficients G_{ij} and G'_{ij} are computed using 4-point Gauss-Legendre quadrature. When $x_i \in \Gamma_j$ the kernels are improper and these coefficients are computed by subtracting the singularity, integrating it analytically and summing with the numerical integral of the remainder.

Upon applying the boundary integral equation to each of the N boundary elements, using the boundary conditions (which specify half of the $2N$ point values of potential and flux), and rearranging, we get the linear system $\mathbf{A}\mathbf{u}_h = \mathbf{f}$ where $\mathbf{u}_h$ contains the unknown potential or flux on the boundary and $\mathbf{f}$ contains the inner product of specified boundary values (i.e., boundary conditions) and kernel coefficients. Once the boundary values are determined, by solving the linear system by Gaussian elimination, the BIE (4.4) can be used to compute the potential at any interior point. The flux vector in the interior can also be computed by operating on (4.4) according to

$$\mathbf{q}(\mathbf{x}) = -\nabla\Phi + \alpha\Phi\nabla z. \tag{4.6}$$

5 Infiltration into Unsaturated Material Above a Deep Water Table

5.1 Specified Moisture

Dimensionless Variables

Here we nondimensionalize variables according to

$$p = \frac{\Phi}{\Phi_o}, \quad \mathbf{x} = \frac{\mathbf{X}}{L} = \frac{(X, Z)}{L}. \tag{5.1}$$

Hence (3.2) becomes

$$\nabla^2 p - a\frac{\partial p}{\partial z} = 0, \tag{5.2}$$

where $a = \alpha L$, and the gradient operator is understood to apply with respect to the nondimensional coordinates (x,z). In addition, the nondimensional flux vector is given by

$$\mathbf{u} = \frac{\mathbf{q}a}{K_o} = -\nabla p + ap\mathbf{e}_z, \tag{5.3}$$

where $K_o = K(\psi_o)$. The boundary conditions on the surface become

$$p = 1, \quad |x| < 1, \quad z = 0, \tag{5.4}$$

$$-\frac{\partial p}{\partial z} + ap = 0, \quad |x| > 1, \quad z = 0, \tag{5.5}$$

and the far-field condition is

$$p \to 0, \quad \mathbf{x} \to \infty. \tag{5.6}$$

We have invoked the approximation that

$$\frac{K(\psi_\infty)}{K(\psi_o)} = \frac{\Phi_\infty}{\Phi_o} = p(\mathbf{x} \to \infty) \ll 1$$

in arriving at the far-field condition. As noted previously, this form of the far-field condition assumes a deep water table and it also assumes a negligible average recharge into the material, other than through the strip. One-dimensional steady recharge through an unsaturated layer, with conductivity as in (1.1), to a water table at $Z = Z_w$ is described by

$$\phi = \frac{q_\infty}{K_s} + \left(1 - \frac{q_\infty}{K_s}\right) e^{\alpha(Z - Z_w)}, \tag{5.7}$$

where $q_\infty > 0$ is the recharge and $\phi = \exp(\alpha\psi)$, as before. For distances above the water table such that $\alpha(Z - Z_w) \ll 0$ the potential approaches q_∞/K_s or

$$\alpha\psi \to \ln\left(\frac{q_\infty}{K_s}\right) \quad \text{as} \quad \alpha(Z - Z_w) \to -\infty,$$

showing that the moisture content approaches a constant value for distances of order α^{-1} above the water table. This condition is assumed in prescribing (2.6) and (5.6) above, together with negligible recharge ($q_\infty/K_s \ll 1$).

If the recharge is not negligible, i.e., $K(\psi_\infty) = O(K(\psi_o))$, then we replace (5.5) with

$$q_z = q_\infty, \quad |x| > 1, \quad z = 0. \tag{5.8}$$

However, if we define

$$p = \frac{\Phi - \Phi_\infty}{\Phi_o - \Phi_\infty} \tag{5.9}$$

then we arrive again at the previous problem, viz., (5.2) subject to (5.4) through (5.6). The only modification is that the flux is now defined by

$$\mathbf{u} \equiv -\nabla p + ap\mathbf{e}_z = a\left(\frac{\mathbf{q} - q_\infty \mathbf{e}_z}{K(\psi_o) - K(\psi_\infty)}\right), \quad \psi_\infty \neq \psi_o. \tag{5.10}$$

Thus, through this definition of variables, the problem is formally reduced to the previous one, although here we solve for the disturbance potential; i.e., the far-field potential has been subtracted off. It is remarkable that, through the quasi-linear transformation, superposition can be applied to a problem that is, in its original form, highly nonlinear.

Results and Discussion

Numerical solutions to this boundary value problem were obtained by applying the boundary integral code described in Section 4 to the transformed versions of the problems discussed above. In these problems the flux is (weakly) singular near $|x| = 1$ in consequence of the step change in boundary condition type. The results given below were computed using the mesh grading algorithm investigated by Yan and Sloan (1989). This technique provides quadratic convergence of the numerical method with systematic reduction in boundary element size. Finally, it is noted that the problem as stated is symmetric with respect to $X = 0$. However, because the numerical method is quite efficient, this symmetry was not exploited, and hence twice as many unknowns were computed than were necessary.

The only parameter appearing in the problem is a $(= \alpha L)$, the nondimensional sorptivity, which is the ratio of the length scale over which capillary effects are active to the breadth of the wetted strip. Large values of α correspond to coarsely graded porous material, (e.g., a bead pack composed of a narrow range of bead sizes or a sandy material), whereas small values of α correspond to well-graded material with a large range of pore size (e.g., loamy soil or some welded tuff). Accordingly, large values of a correspond to well-sorted porous material or to a relatively large wetted area on the surface. Hence, the distribution of moisture beneath the wetted source will be gravity-dominated for large a, and the wetted lobe is expected to be in the form of a highly elongated "finger." Conversely, the wetted lobe is expected to be broadly spread for small a, where capillary effects manifest themselves.

This description of the potential (or moisture) distribution is borne out in the solutions as illustrated in Figures 5.1 through 5.3, showing contour plots of the potential p for $16^{-1} \leq a \leq 16$. Gravity acts in the direction of increasing z in these figures. The contours approach a circular form as $a \to 0$, as described earlier. However, even for small values of a, the contours for the smaller values of potential (e.g., $p < 0.4$ in Figure 5.1a) become increasingly elongated showing that the body force is always dominant far from the source. Higher values of the contours approach a circular form near the source. The broad spread of the contours decreases with increasing a, and the contours take a highly elongated form, in the vertical direction, for large a. Figure 5.2b for $a = 1$ already shows that most of the contours take on a "finger–like" form, although contours near the source must return to a more circular form in consequence of the surface boundary condition. Thus, for large a, the moisture introduced at the surface falls nearly vertically with little lateral diffusion.

For $a \to 0$, the boundary value problem becomes increasingly of the potential type, satisfying Laplace's equation. There are no solutions for $a = 0$, however, because of the no-flux boundary on the surface for $|x| > 1$. This is easily seen by referring to the conformal mapping indicated in Figure 5.4. In the (u, v) domain, the potential must go linearly from unity at $v = 0$ to zero at infinity, an untenable requirement. The approach to this solution is evident in Figures 5.1 for $a \ll 1$. Consider the contour level 0.5 in Figures 5.1 through 5.3 for example: the physical extent of this level is minimum for $a \approx 1/2$, while for larger values the depth to this contour level increases along the symmetry line, $x = 0$. However, for smaller values of a the level also increases in extent, more or less uniformly with respect to the origin. Mapping Figure 5.1a through c conformally, according to Figure 5.4 for example, would show the approach to a linear profile for the potential for decreasing a.

For large a, capillary effects are significant only near the source, and, as was shown by Weir (1986) in a similar problem, for $a \to \infty$ capillary effects are significant only near $(x, z) = (\pm 1, 0)$. This is illustrated in Figures 5.3b and c, for example, showing the isopotentials emanating from this location. Futhermore, when $a \to \infty$, the potential is asymptotically governed by a heat equation as shown by Weir (1986),

$$\frac{\partial^2 p}{\partial x^2} - a\frac{\partial p}{\partial z} = 0$$

with diffusivity a^{-1}. This equation represents the lowest-order problem in an asymptotic outer expansion for large a. This is an outer expansion since this form is not uniformly valid, due to neglect of the vertical diffusion term in the field equation for the potential, (5.2). The asymptotic equation represents a balance of horizontal diffusion and vertical buoyancy-driven flow and is equivalent to the high Peclet number limit in a convection-diffusion equation. The boundary conditions remain the same, except that (5.5) is replaced with

$$p = 0, \quad |x| > 1, \quad z = 0, \tag{5.11}$$

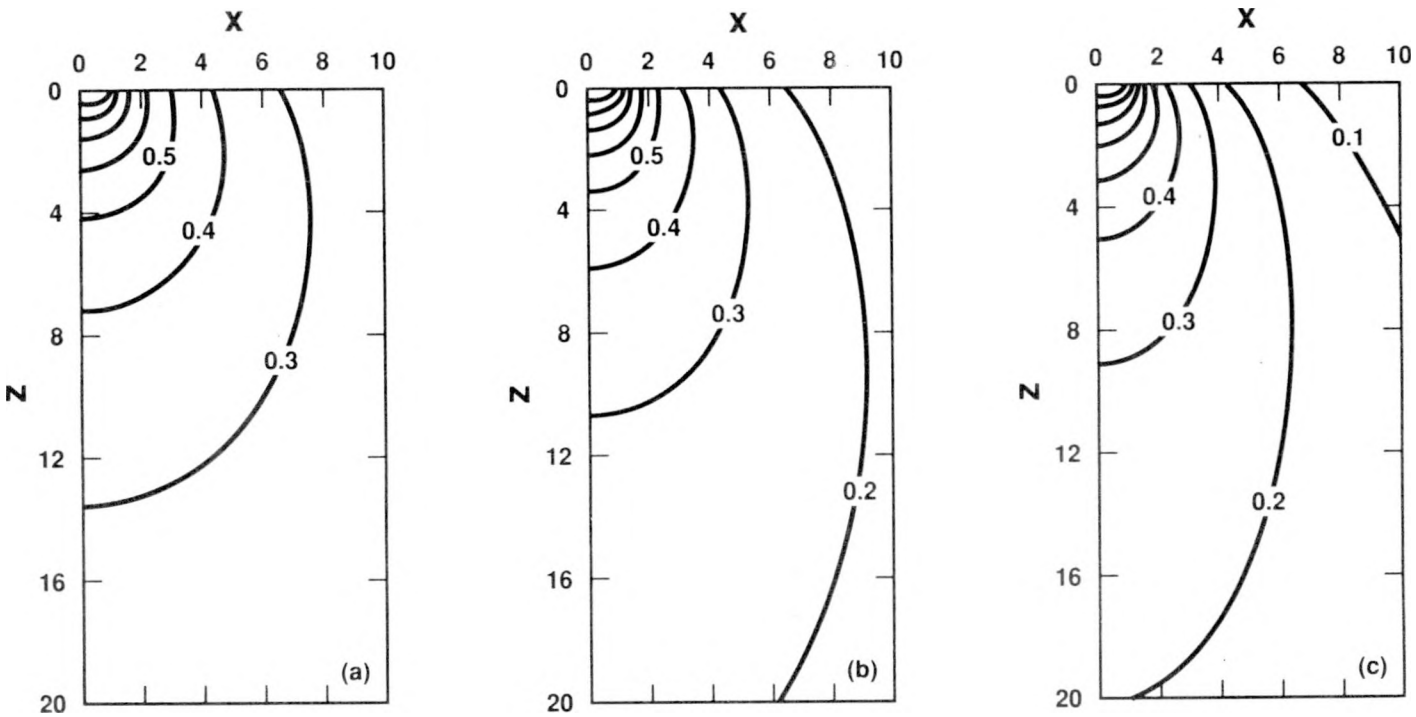

Figure 5.1. Isopotentials for various values of the nondimensional sorptivity. Gravity acts along the direction of increasing z; (a) $a = 16^{-1}$, (b) $a = 8^{-1}$, (c) $a = 4^{-1}$.

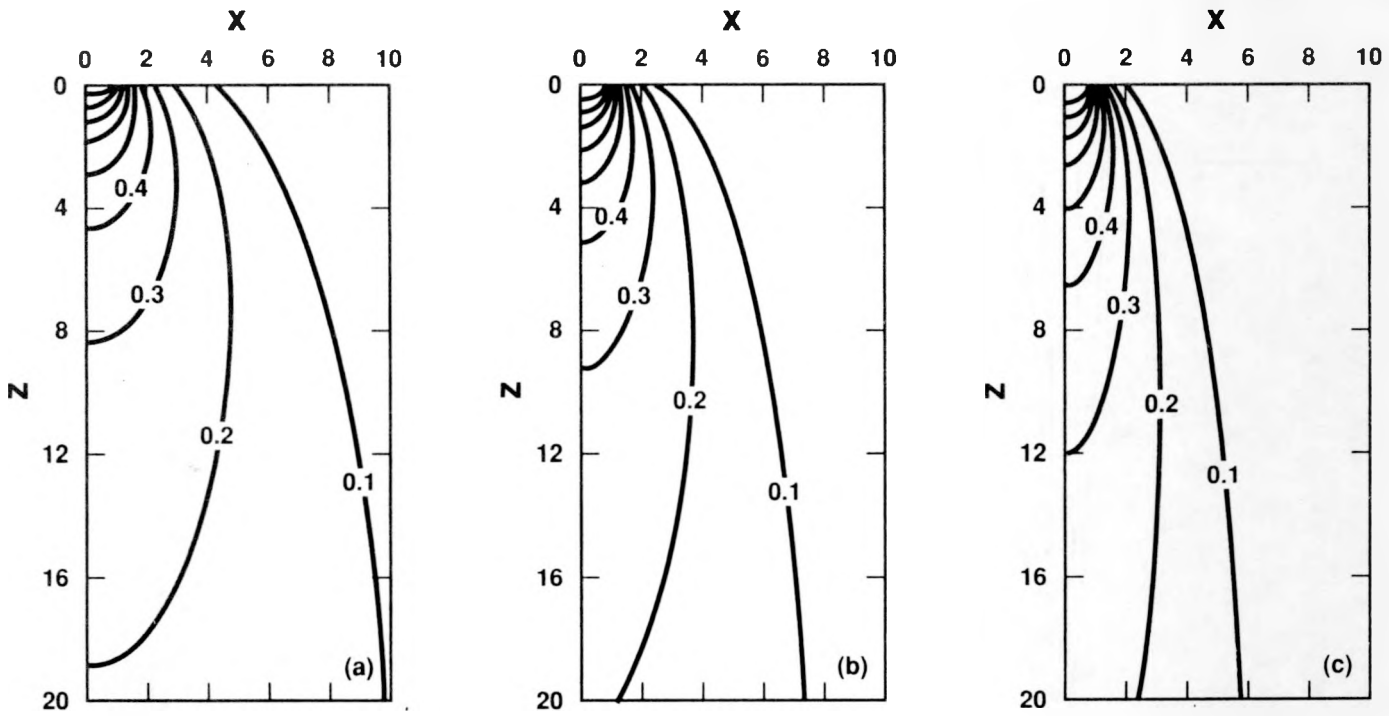

Figure 5.2. Isopotentials for various values of the nondimensional sorptivity. Gravity acts along the direction of increasing z; (a) $a = 2^{-1}$, (b) $a = 1$, (c) $a = 2$.

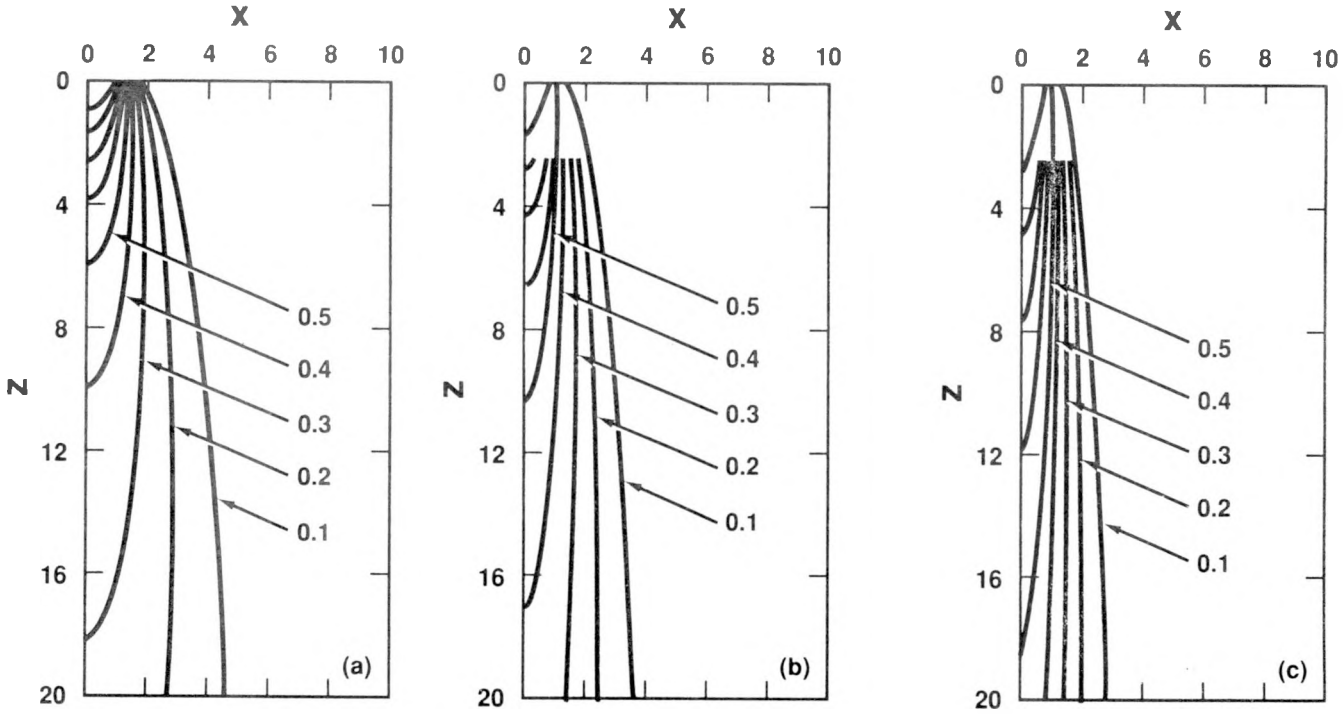

Figure 5.3. Isopotentials for various values of the nondimensional sorptivity. Gravity acts along the direction of increasing z; (a) $a = 4$, (b) $a = 8$, (c) $a = 16$.

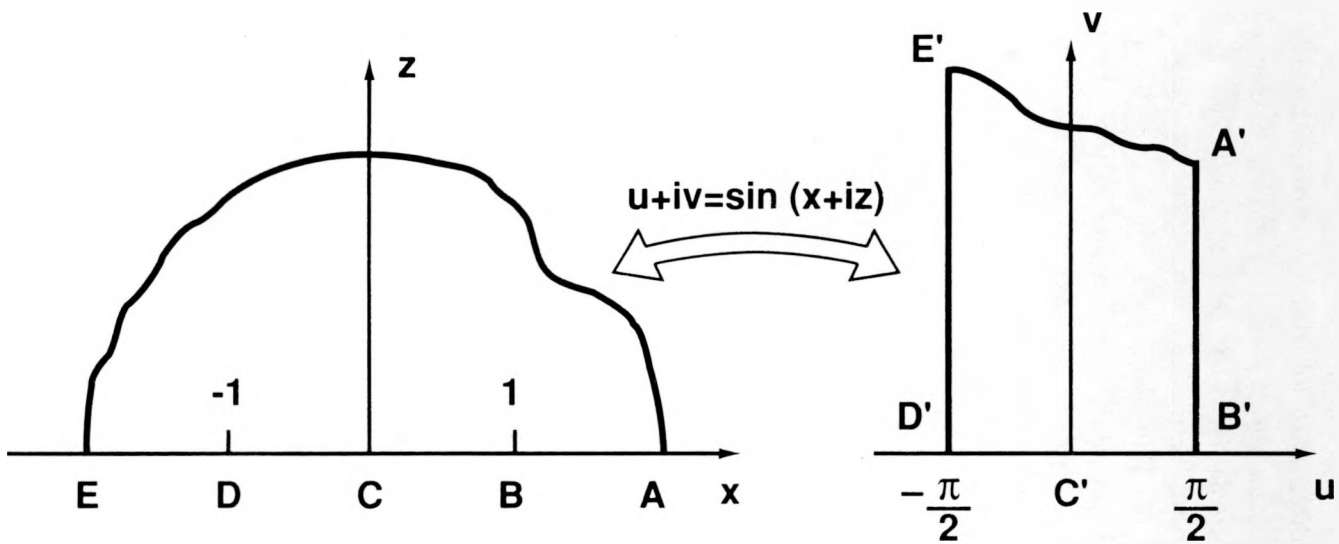

Figure 5.4. Conformal mapping of the analogous potential problem. This is Figure 9 in Appendix 2 of Churchill, *et. al.* [29]

since vertical diffusion is asymptotically smaller than the gravity term for large a. The solution to this heat equation (Carslaw and Jaeger, 1978, p. 55), is given by

$$p = \frac{1}{2}\left(\text{erf}\frac{1-x}{2\sqrt{z/a}} + \text{erf}\frac{1+x}{2\sqrt{z/a}}\right).$$

Contours of p for this approximate solution are shown in Figure 5.5 for $a = 8$ and 16. The comparison with Figures 5.3b and c is quite good except near the plane $x = 0$ where the asymptotic solution underestimates the penetration of the potential by a slight amount. This is further illustrated in Figure 5.6 showing the potential variation with depth along the symmetry line, $x = 0$. The discrepancy between the asymptotic solution and the full solution will be greatest along this line because of the neglect of vertical diffusion in the asymptotic solution. Indeed, the asymptotic solution is seen to lag along $x = 0$ in Figure 5.6a; otherwise the comparison is excellent. It is also of interest to point out the very slow decay of the potential from unity at the source to the far-field value as indicated in Figure 5.6b. This slow decay affirms the utility of the boundary integral method for half-plane problems. Use of a finite difference or finite element technique would require either a very large domain to satisfy the far-field condition, or the use of solution approximations on a truncated domain. In general, the latter technique requires some knowledge of the solution behavior in the far field.

The variation of potential and vertical infiltration flux along the surface, $z = 0$, is shown in Figures 5.7 and 5.8, respectively, for some selected values of a. The moisture diffuses away from the source for a substantial distance for small a. On the other hand, the potential decreases rapidly along the surface when $a \gg 1$, as assumed in the boundary condition (5.11) for the asymptotic problem discussed above. The step change in boundary condition at $|x| = 1$ results in a singularity in the surface flux at that point, as shown in Figure 5.8. The singularity becomes increasingly localized about $|x| = 1$ as $a \to \infty$; the profile for $a = 16$ shows almost constant flux except in a region very near this point. Physically, this singularity models the large lateral gradient in potential near this transition from specified potential to a no-flux surface.

The nondimensional flux through the surface is given by

$$F_o = 2a\frac{\bar{q}_o}{K_o}, \tag{5.12}$$

where

$$\bar{q}_o = \frac{1}{L}\int_0^L q_z(X, Z = 0)dX.$$

Computed values are given in Table 5.1 and plotted in Figure 6.3 as the curve labeled $d = \infty$. As was shown by Weir (1986), the flux is accurately described by the simple relation,

$$F_o^* = 2a + \frac{4}{\pi},$$

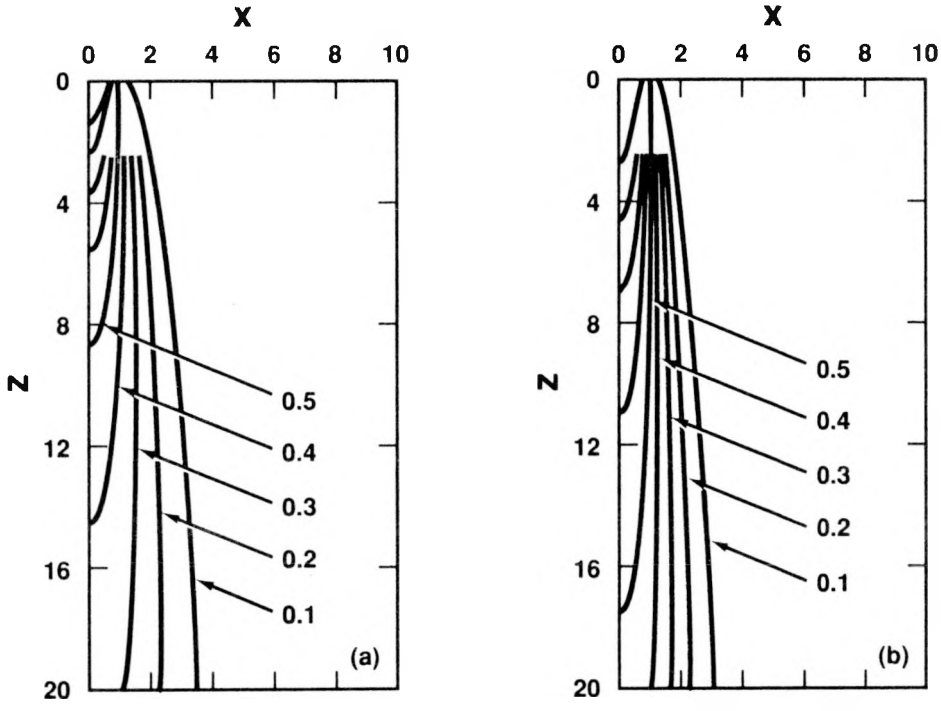

Figure 5.5. Isopotentials of p given by the asymptotic solution for large a, (a) $a = 8$; (b) $a = 16$.

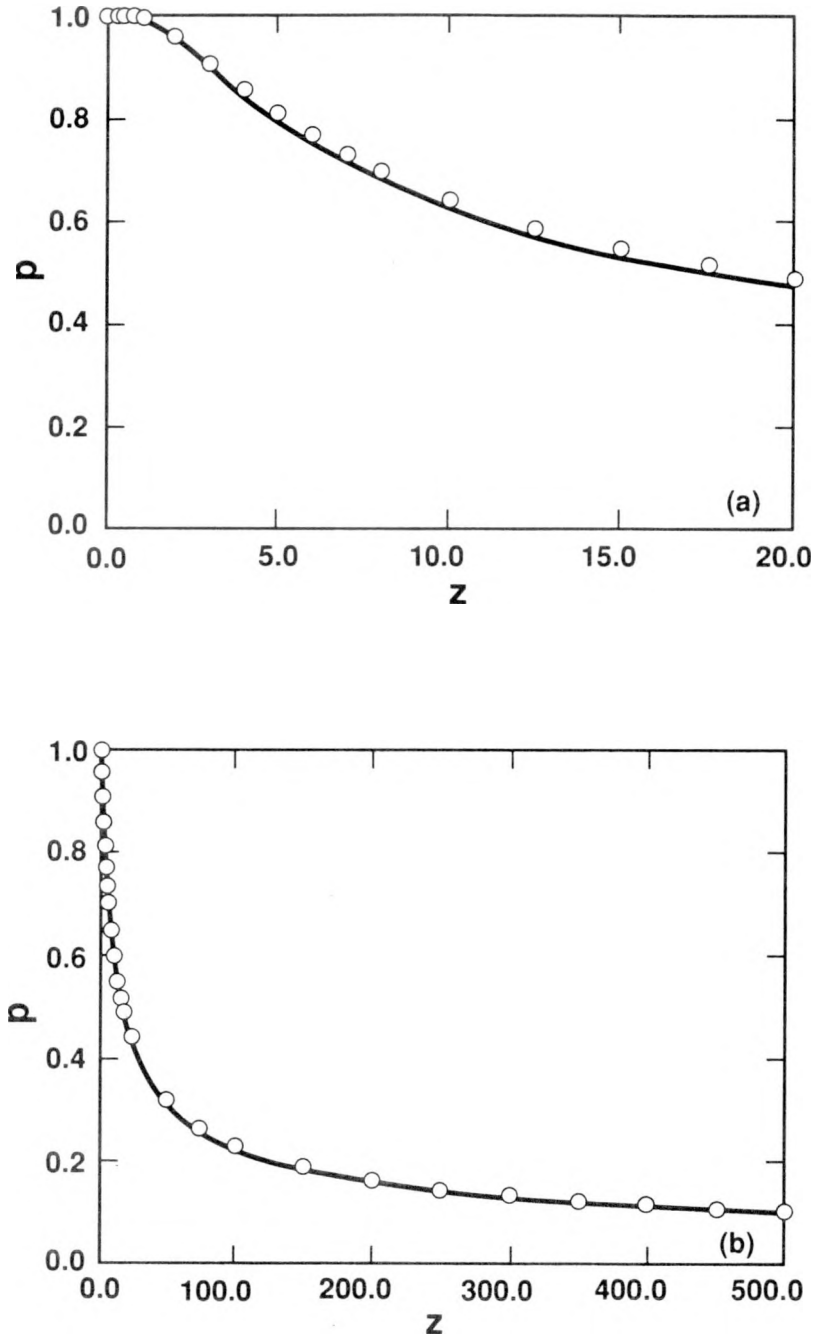

Figure 5.6. Comparison between the asymptotic solution (solid curve) and the boundary integral solution (symbols) for the potential profile along $x = 0$ for a=16. Figure 5.6a shows that the asymptotic solution lags the numerical solution and Figure 5.6b illustrates the slow decay of the potential far from the source.

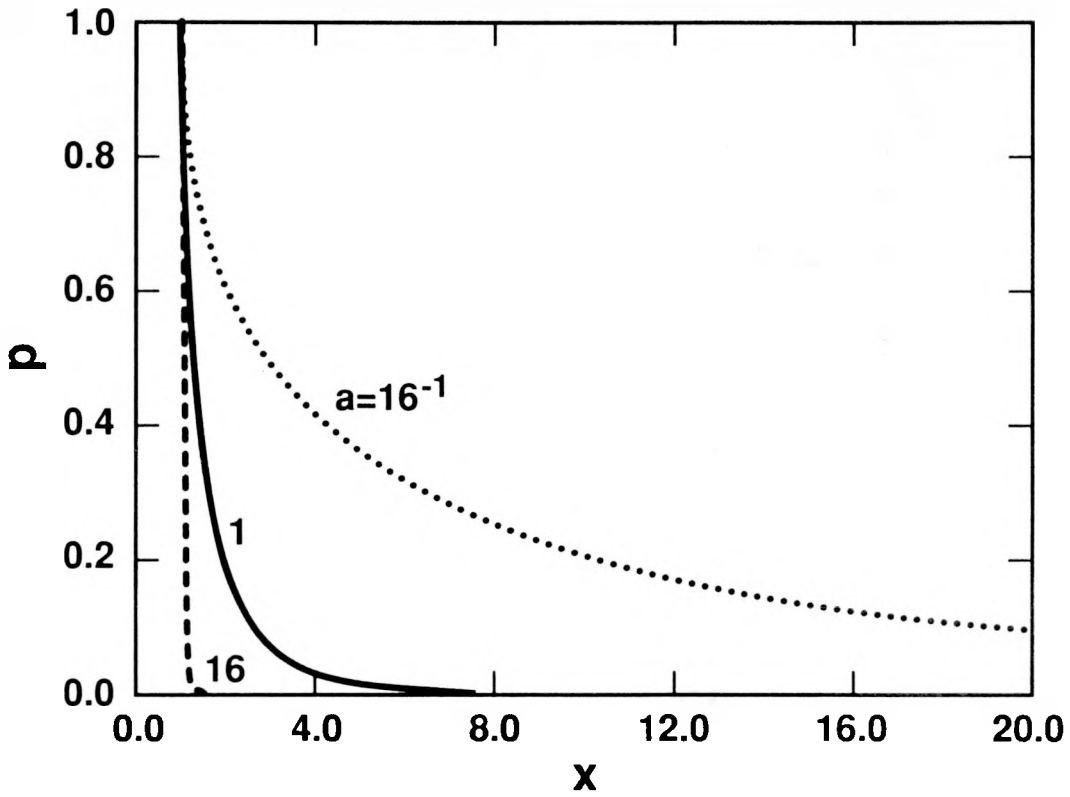

Figure 5.7. Profiles of potential along the surface ($z = 0$) for various values of $a = \alpha L$, for the Dirichlet source.

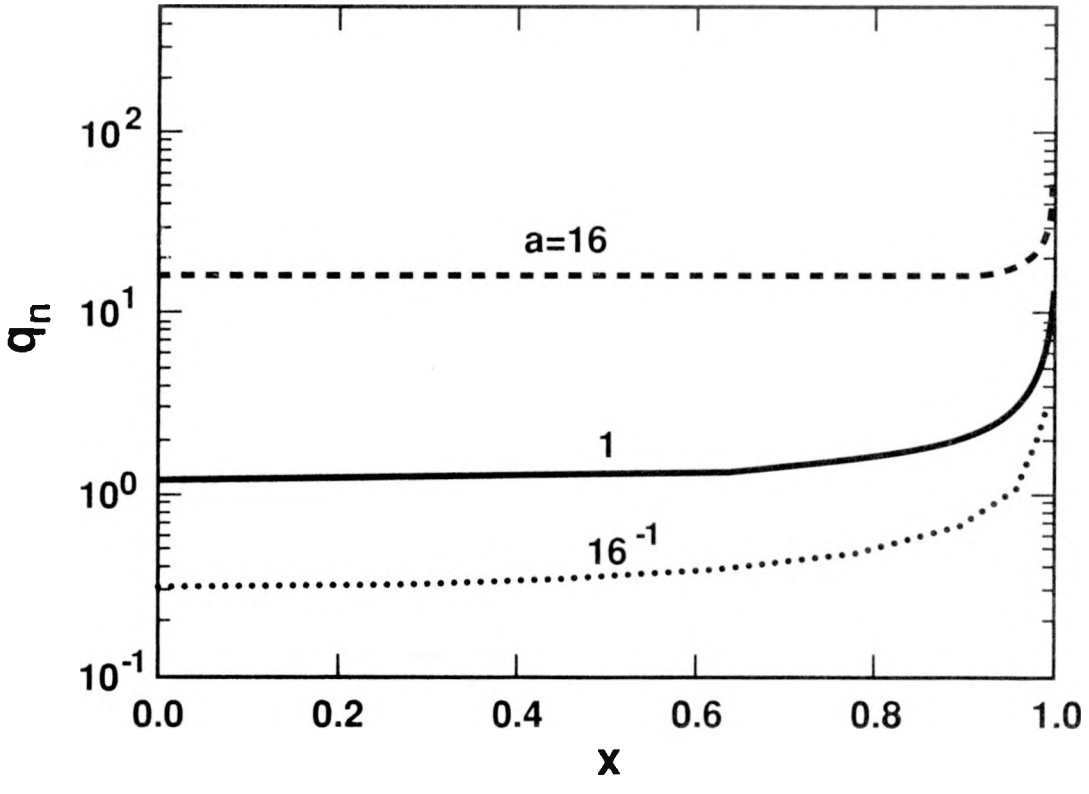

Figure 5.8. Profiles of infiltration flux along the surface ($z = 0$) for various values of $a = \alpha L$, for the Dirichlet source.

Table 5.1. Nondimensional Flux

αL	F_o	$\bar{q}_o/K_s$	$(F_o^* - F_o)/F_o^*$
16^{-1}	0.9469	7.575	3.23×10^{-1}
8^{-1}	1.181	4.723	2.25×10^{-1}
4^{-1}	1.543	3.087	1.30×10^{-1}
2^{-1}	2.146	2.146	5.60×10^{-2}
1	3.224	1.612	1.50×10^{-2}
2	5.257	1.314	3.08×10^{-3}
4	9.265	1.158	8.89×10^{-4}
8	17.26	1.079	7.66×10^{-4}
16	33.26	1.039	3.98×10^{-4}
32	65.21	1.019	9.69×10^{-4}

for large a. The numerical results show this relation is accurate for $a > 1$, and is in error by at most 6% for $0.5 < a < 1$. It is also of interest to note that the average Darcy flux through the wetted strip, $\bar{q}_o$, approaches K_o for $a \gg 1$ (Table 5.1). When the moisture level at the source is saturated, i.e., $\psi_o = 0$, and $K_o = K_s$, the results indicate that the net infiltration approaches the saturated conductivity for large a. This is not surprising because, for gravity dominated flow, the material can transport fluid only at about the rate of the saturated conductivity and still remain unsaturated everywhere (except at the source if $\psi_o = 0$). For small values of a, however, the material can absorb at a rate many times K_s, and still remain unsaturated. This is because capillary forces are able to spread the moisture laterally as well as vertically, allowing the material to absorb at a high rate, compared to the saturated conductivity.

5.2 Specified Flux

Dimensionless Variables

If the flux of moisture is to be specified rather than the moisture itself, we replace the condition (2.2) with (2.4) while conditions (2.3) and (2.6) remain as before. We also use the same nondimensional variables as before, expressed in (5.1), except we define

$$\alpha \Phi_o = q_o. \tag{5.13}$$

The nondimensional field equation for the potential is again (5.2) and the flux is given by (5.3), if we replace K_o with q_o in the latter. The boundary condition at the source is now given by

$$-\frac{\partial p}{\partial z} + ap = a, \quad |x| < 1, \quad z = 0, \tag{5.14}$$

and the impermeable condition is again (5.5) and the far-field condition is (5.6). In terms of these nondimensional variables, the problem is again parameterized entirely by

the nondimensional sorptive length, a, although the dimensionless potential is measured here in terms of the applied flux.

Results and Discussion

These nondimensional variables render this problem in a form very similar to the previous problem. Indeed, the solutions for various values of a are also similar, both qualitatively and quantitatively, if the potential were rescaled, to their counterparts for the Dirichlet problem. For example, a contour plot of potential for a given value of a can be made to match reasonably well with a corresponding solution for which the moisture is specified on the strip, if the potential in the present problem were rescaled such that $p(0,0) = 1$. The variation of potential along the surface is shown in Figure 5.9 for some selected values of a. Again, these profiles exhibit a similar relation to a as compared to their counterparts for the Dirichlet source, shown in Figure 5.8, if the potential is scaled such that $p(0,0) = 1$. Indeed, the lateral diffusion of potential is substantial when $a \ll 1$, and the potential profiles approach the approximation (5.11) made for the large a asymptote for the Dirichlet problem. Comparison of our results with the solutions for $a = 0.2$ and 0.5 presented by Batu (1978) is good, i.e. within the error introduced in extracting points from the contour plots of potential shown in Figure 3 of (Batu, 1978).

Implicit in the quasi-linear analysis is that $\psi \leq 0$ everywhere in the solution domain. Obviously, for given a, there is a unique q_o, above which this condition is violated. The limit on the capillary potential can also be expressed as, $\Phi \leq K_s/\alpha$, or in terms of dimensionless variables, $p \leq K_s/q_o$. Hence, for given a, the maximum flux the material can transport and yet remain unsaturated below the source is

$$\frac{q_o^*}{K_s} = \frac{1}{p^*} \tag{5.15}$$

where p^* is the maximum value of potential in the half-plane $z \geq 0$ determined for the boundary condition (5.14). Any flux greater than q_o^* will produce a saturated bulb beneath the source. In consequence of the symmetry in the current problem (and also in the Dirichlet problem), $p^* = p(0,0)$. Values of the maximum flux are listed in Table 5.2 and plotted in Figure 6.7 (curve labeled $d = \infty$) as a function of a. These maximum values are slightly lower than the corresponding flux values in Table 5.1 for the Dirichlet source; however, their relationship with a is similar.

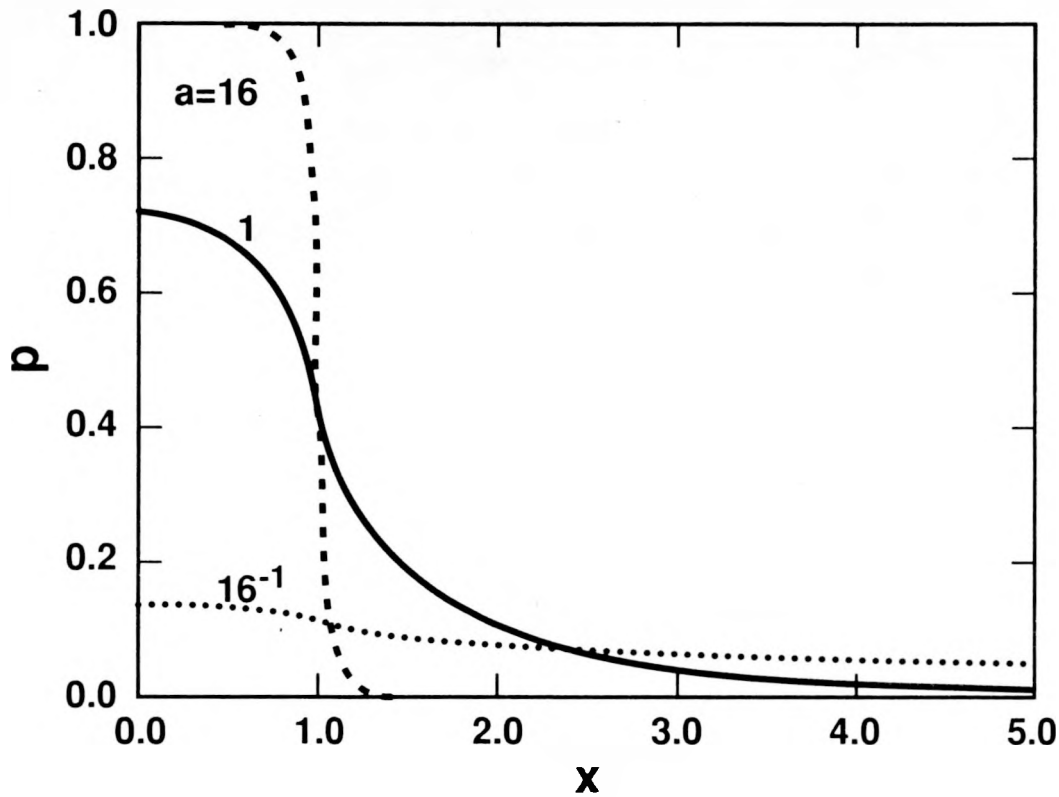

Figure 5.9. Profiles of potential along the surface ($z = 0$) for various values of $a = \alpha L$, for the specified flux source.

Table 5.2. Maximum Flux for Unsaturated Flow.

αL	p^*	q_o^*/K_s
16^{-1}	0.1435	6.968
8^{-1}	0.2337	4.278
4^{-1}	0.3643	2.745
2^{-1}	0.5345	1.871
1	0.7237	1.382
2	0.8849	1.130
4	0.9743	1.026
8	0.9982	1.002
16	1.0002	0.9998

6 Infiltration into Unsaturated Material Above a Shallow Water Table

6.1 Specified Moisture

Dimensionless Variables

We use the same dimensionless variables defined for the case of a deep water table, viz., Equation (5.1), except we replace Φ_o, with Φ_s, the value of potential at the water table,

$$\alpha\Phi_s = K_s. \tag{6.1}$$

The field equations for potential and flux are again (5.2) and (5.3), respectively, replacing K_o with K_s in the latter equation. The surface boundary conditions are

$$p\,(=\frac{\Phi}{\Phi_s}) = p_o, \quad |x| < 1, \quad z = 0, \tag{6.2}$$

and (5.5) over the remainder of the surface. The boundary condition on the water table is

$$p = 1, \qquad \text{for all } x,\ z = d. \tag{6.3}$$

Because the boundary integral formulation requires that $p \to 0$ as $\mathbf{x} \to \infty$, it is convenient to solve for the disturbance potential, representing the deviation from the capillary fringe solution. Thus, we write

$$p = p' + p^\infty, \tag{6.4}$$

where p^∞ satisfies

$$q^\infty = -\frac{dp^\infty}{dz} + ap^\infty = 0,$$

subject to $p^\infty = 1$ when $z = d$. Thus,

$$p^\infty = e^{a(z-d)}. \tag{6.5}$$

The disturbance potential, p', satisfies the operator in (5.2) subject to

$$p' = p_o - e^{-ad}, \quad |x| < 1, \ z = 0, \tag{6.6}$$

$$u'_z = -\frac{\partial p'}{\partial z} + ap' = 0, \ \ |x| > 1, \ \ z = 0, \tag{6.7}$$

$$p' = 0, \text{ for all } x, z = d. \tag{6.8}$$

In the investigations to follow, only a saturated source is considered, i.e., $p_o = 1$. However, because the remaining boundary conditions on the disturbance potential are homogeneous, solutions for arbitrary values of p_o can be obtained from the solutions determined herein for $p_o = 1$ by rescaling the disturbance potential, thus eliminating p_o as a parameter. Hence, consideration of a shallow water table introduces two additional parameters in the problem; these are the dimensionless depth to the water table, $d = D/L$, and $ad = \alpha D$, which modifies the source strength for the disturbance potential.

The boundary condition on the strip source, (6.6), suggests the length scale over which the water table will affect the potential field. If $ad \gg 1$ (actually, if $ad > 2$, say), the capillary fringe thickness is small and the boundary value at the source for the disturbance potential is unaffected by the capillary fringe. The infiltration is also unaffected, relative to results for the deep water table when $ad \gg 1$ as shown in the following. In this case we say that the water table is 'deep' below the surface, and the boundary value problem for the disturbance potential is nearly identical to the problem discussed in Section 5.1, except here the capillary fringe is superposed over a distance of $O(\alpha^{-1})$ above the water table.

The boundary value problem for the disturbance potential is solved numerically via the boundary integral equation method discussed above. In this problem, the line $z = d$ is discretized along with the surface, $z = 0$. The lateral extent of the mesh on these lines depends on a and on d, although to a weaker degree. The lateral extent was as much as $|x| = 300$ for $a = 32^{-1}$ and as small as $|x| = 2$ for $a = 16$. The full solution is given by superposing the numerical results with (6.5).

Results and Discussion

The influence of the depth to the water table depends on the nondimensional sorptivity for the material, as illustrated in Figure 6.1, which shows contours of potential, $p = p' + p^\infty$, for various values of a and fixed depth. These figures can be compared to the corresponding plots for a deep water table, Figures 5.1 through 5.3. For $a = 16$, the distribution of potential is virtually identical to the distribution for the deep water table, Figure 5.3c, except for the boundary layer adjustment for distances $O(\alpha^{-1})$ above the

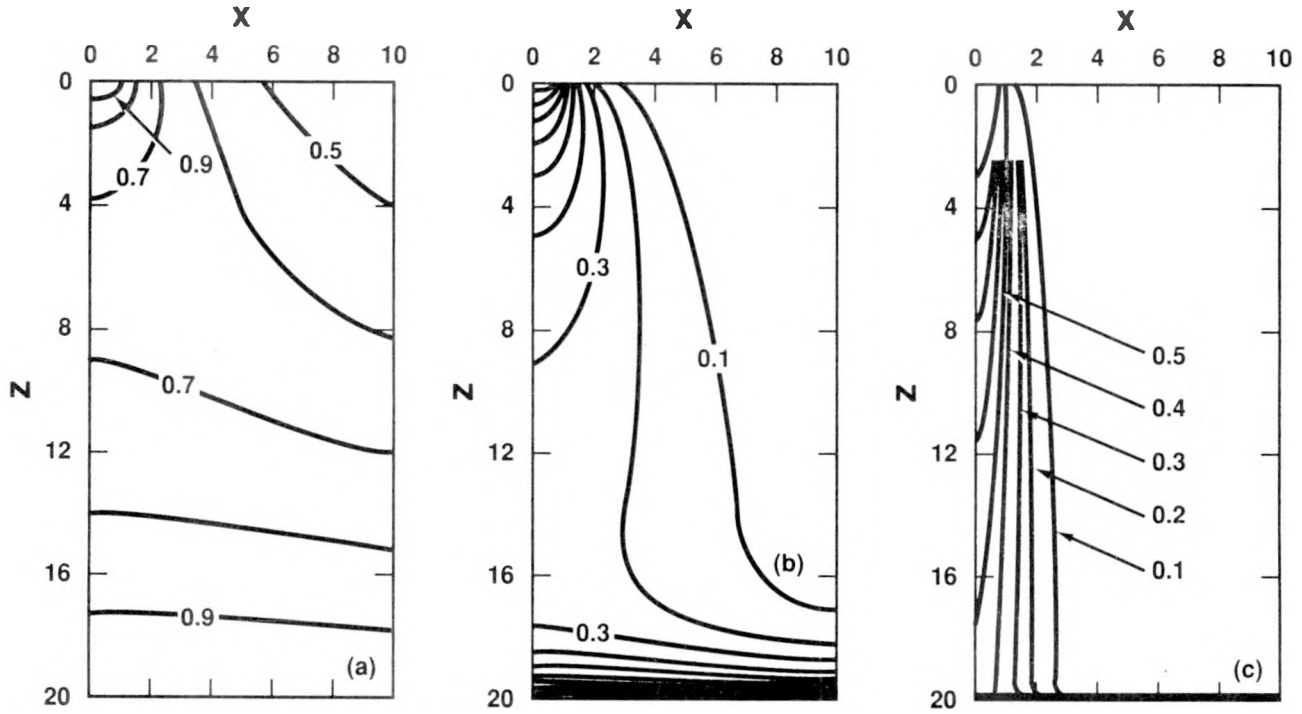

Figure 6.1. Isopotentials for $d = 20$ and (a) $a = 16^{-1}$, (b) $a = 1$, and (c) $a = 16$.

water table. This is the characteristic thickness of the capillary fringe, as indicated in Equation (6.5). The capillary fringe thickens for decreasing a and fixed d as illustrated in Figure 6.1. For $a = 1$, the contours are still similar to those for $d \to \infty$ (shown in Figure 5.2b) for $z < 15$ but deviate for locations closer to the water table. Finally, for $a = 16^{-1}$, the dimensionless capillary fringe thickness is $O(16)$ and the potential distribution departs significantly from those for the deep water table, the presence of the shallow water table resulting in much a wetter material throughout. For example, in Figure 5.1a the lowest contour level is 0.3, while in Figure 6.1a, contours lower than 0.5 are not present in the domain shown. Similar conclusions can be drawn from Figure 6.2, showing contours of potential for $d = 1$ and $a = 1$ and 16. The capillary fringe occupies only a thin boundary layer above the water table when $a = 16$, while the capillary fringe pervades the entire depth of material when $a = 1$. A contour plot for $a = 16^{-1}$ is not included because the layer of material is at a potential higher than 0.93 throughout. The dominance of gravity flow over diffusion of moisture is strikingly displayed in Figure 6.2b indicating nearly vertical flow of moisture, resulting in the region $|x| < 1$ being nearly saturated while the region $|x| > 1$ is relatively dry, these regions being separated by a diffusion zone which thickens with depth. Even at this shallow depth, however, the capillary fringe is too thin to have any effect on the net infiltration into the source area for $a = 16$; the computed value of F_o for this case agrees with the value computed when $d \to \infty$ to five significant figures.

The effects of variation in a and d on the average dimensionless infiltration through the source, F_o, are summarized in Figure 6.3. F_o is defined in Equation (5.12). The results from Section 5.1 are included as the curve labelled $d = \infty$. The shallow water table influences the infiltration only for smaller values of a. If a is sufficiently large, gravity flow dominates and the capillary fringe is thin compared to the depth d and the infiltration is unaffected. The infiltration is independent of d for $a > 5$ (in the range of d considered in Figure 6.3) and is proportional to a as discussed by Weir (1986). The figure also illustrates that influence of the water table is manifest when $ad = O(1)$; thus, for a given material type and source width (αL), the water table affects the infiltration if $D = O(\alpha^{-1})$. This is evident in Figure 6.3 where, for given d, the deviation from the deep water table results begins roughly when $ad \approx 4$. Moreover, the value $ad = 2$ is where the capillary fringe reduces p' in (6.6) by about 10% ($p_o = 1$). For larger ad, the infiltration is given, with good accuracy, from the results assuming $d \to \infty$. For fixed a, Figure 6.3 shows that the infiltration is a monotonically increasing function of d; the maximum flux is given by the deep water table results ($d = \infty$).

The distribution of vertical flux at the water table is shown in Figure 6.4 as a function of nondimensional depth and sorptivity. The maximum flux occurs on the symmetry axis, $x = 0$, and is approximately proportional to a. The effect of increasing depth, for fixed a, is to spread the flux distribution at the water table. Conversely, as the depth decreases, the flux is more closely confined to the region about the symmetry axis. The spreading also increases with decreasing a, for fixed d, as diffusion becomes important

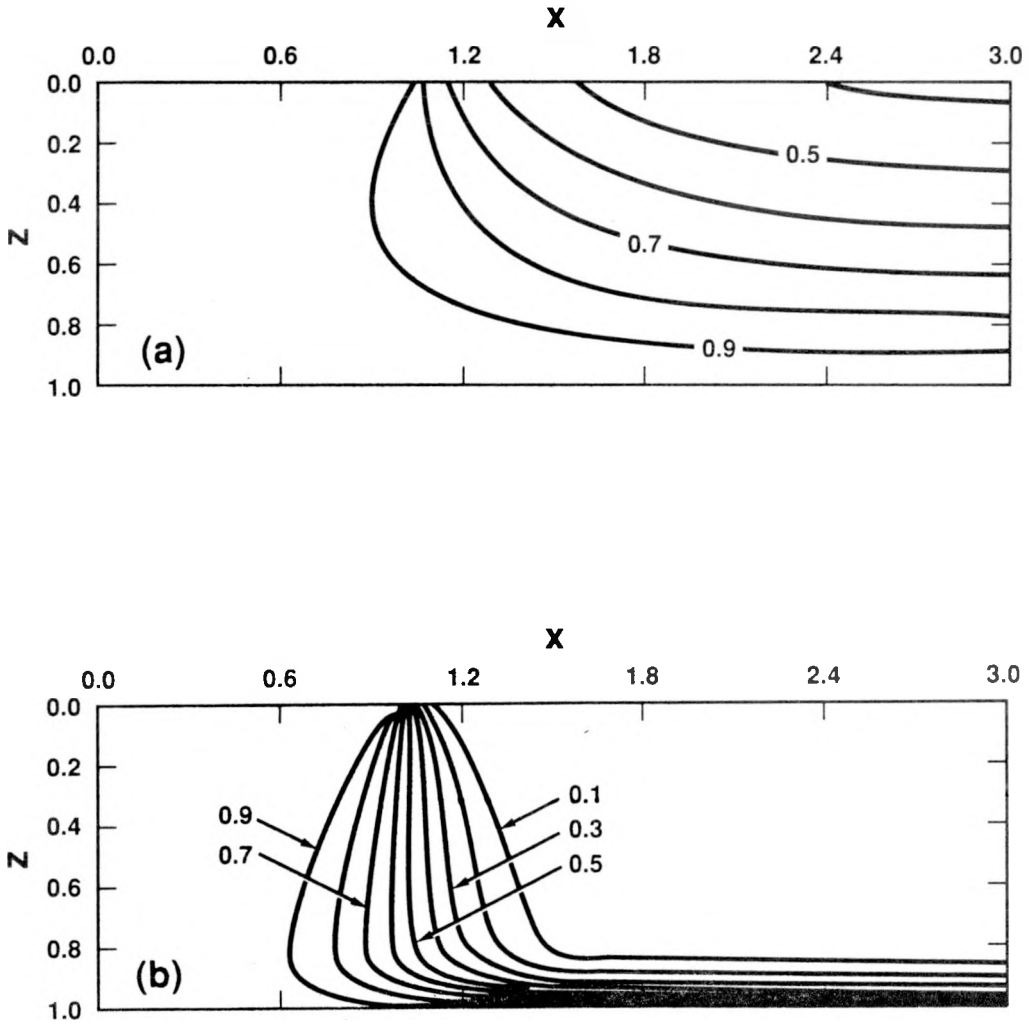

Figure 6.2. Isopotentials for $d = 1$ and (a) $a = 1$, and (b) $a = 16$.

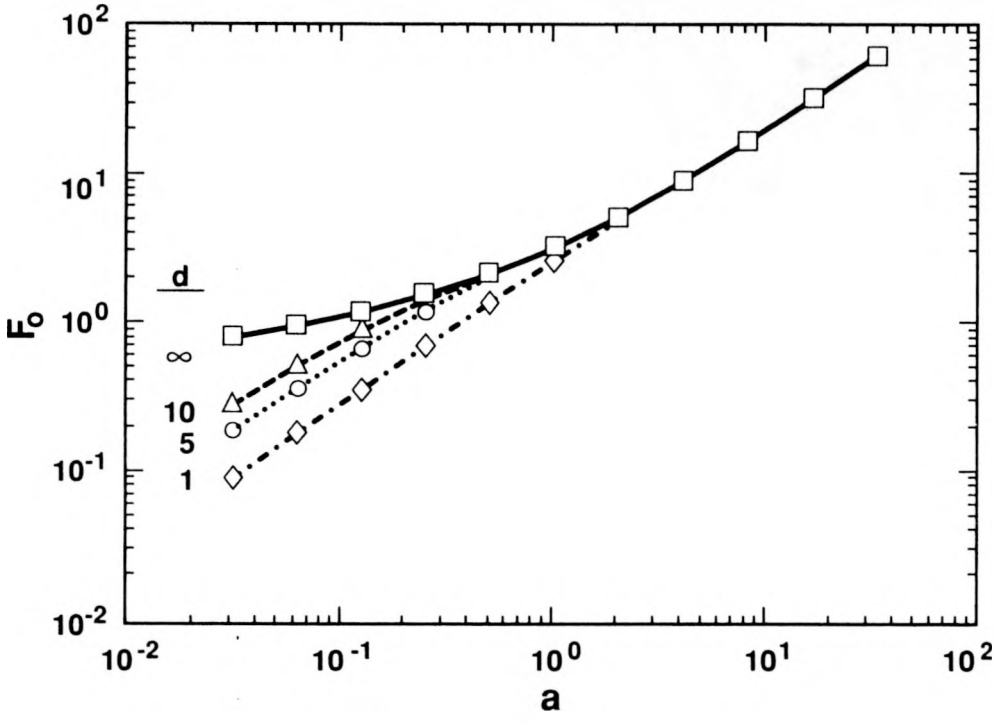

Figure 6.3. Variation of the total infiltration through source area with nondimensional sorptivity, $a = \alpha L$, and depth to the water table, $d = D/L$.

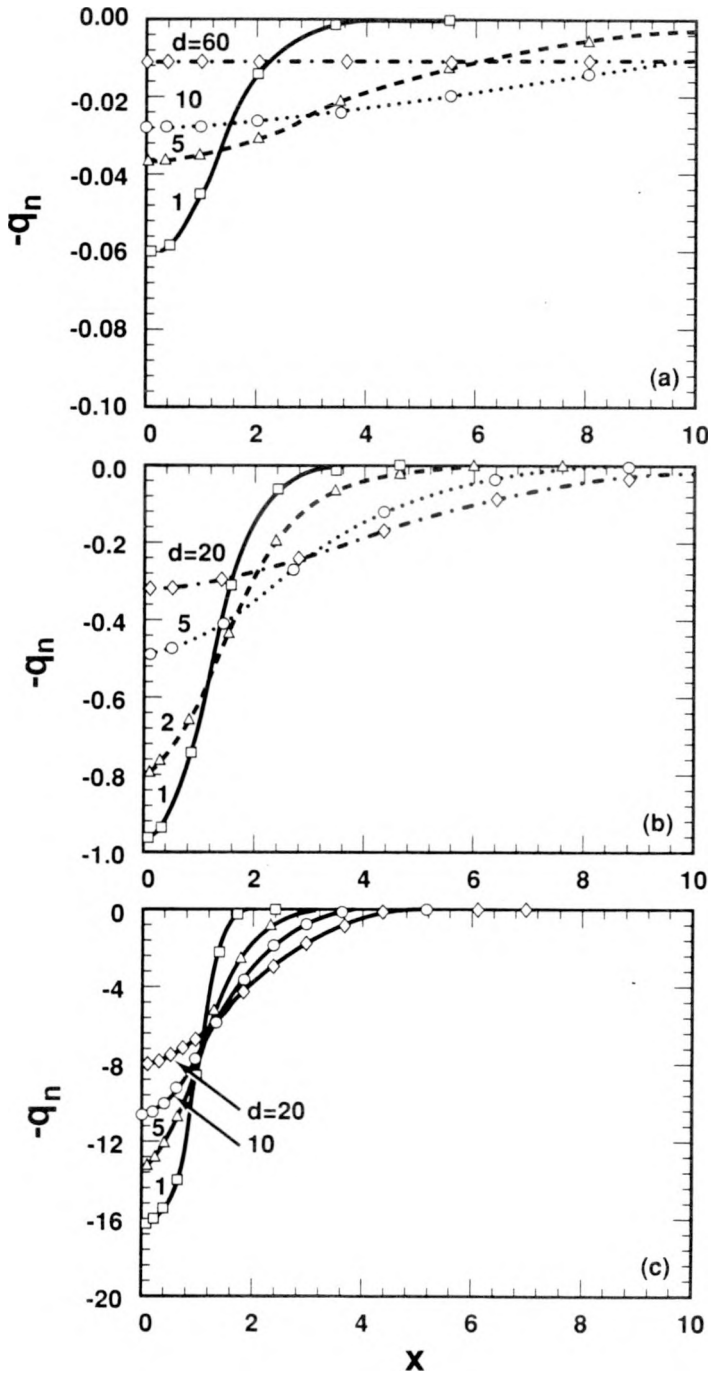

Figure 6.4. The normal flux (scalar product with the outward pointing normal) at the water table for various values of depth from the surface and (a) $a = 16^{-1}$, (b) $a = 1$, and (c) $a = 16$.

and finally dominant for $a \to 0$. This is especially notable in Figure 6.4a for $d = 60$. The distribution of flux is nearly constant on the scale shown, and the numerical mesh included the portion of the line $|x| = 250$ on both $z = 0$ and $z = d$ in order to extend the mesh into the undisturbed region. This is another example of the utility of the current technique over domain methods (e.g., finite difference or finite element) for problems which are semi-infinite in extent. Such an increase in the size of the computational domain would greatly increase the number of unknowns for a domain method, since the mesh would have to be extended in two-dimensions rather than simply along a line as in the present method.

The spreading of moisture introduced at the source is also illustrated by computing the pathline taken by a fluid particle introduced at the source. Pathlines are computed by numerically integrating the equations

$$\frac{d}{dt}\begin{pmatrix} x \\ z \end{pmatrix} = \begin{pmatrix} v_x \\ v_z \end{pmatrix} = \frac{1}{\theta}\begin{pmatrix} q_x \\ q_z \end{pmatrix}$$

for each pathline, subject to an initial coordinate location, (x_o, z_o). The fluxes are given by (5.3), and the moisture content must be specified as a function of pressure head. For purposes of illustration in the examples shown, the moisture content was set to unity, thereby allowing computation of the particle path, although the travel time cannot be correctly obtained. If $\theta(\psi)$ is specified, the pressure head can be calculated from Equations (6.4), (5.1), and (3.3). Hence, the interstitial velocity, $\mathbf{v}$ $(=\mathbf{q}/\theta)$, can be obtained from the flux vector, thereby allowing evaluation of the elapsed time for the particle to travel along the path.*

The lateral diffusion of moisture in its travel towards the water table is illustrated in Figure 6.5 for $a = 16^{-1}$ and 1; Figure 6.6 shows the same results over a larger domain. The lateral spreading increases with decreasing sorptivity and is substantial when $a = 16^{-1}$. The particle that departs from $(x_o, z_o) = (1.5, 0.1)$ near the surface moves laterally to $x \approx 100$ before arriving at the same depth below the surface (see Figure 6.6). By contrast, when $a = 1$, the lateral dispersion of the same particle is only about one–fourth this value at a depth $z = 100$. Hence, the lateral dispersion decreases as a increases because gravity comes to dominate diffusion. The depth to the water table also influences the particle dispersion, but this effect is dependent on a as well. When the water table is at a depth of 20 units of L below the surface, the lateral displacement of the particle for $a = 16^{-1}$ is about $x \approx 30$, compared to $x \approx 44$ for $d \to \infty$. For $a = 1$, however, the water table influence is much reduced and the lateral displacements of pathlines for $d = 20$ are virtually identical to those for a deep water table.

Once again, the influence of the water table on the pathlines is characterized in terms of the characteristic capillary fringe thickness, ad. The presence of the water table

*If only the pathline is desired, without regard for the travel time, it is computationally expedient to integrate the single equation $dz/dx = v_z/v_x$ for each pathline rather than the pair indicated above.

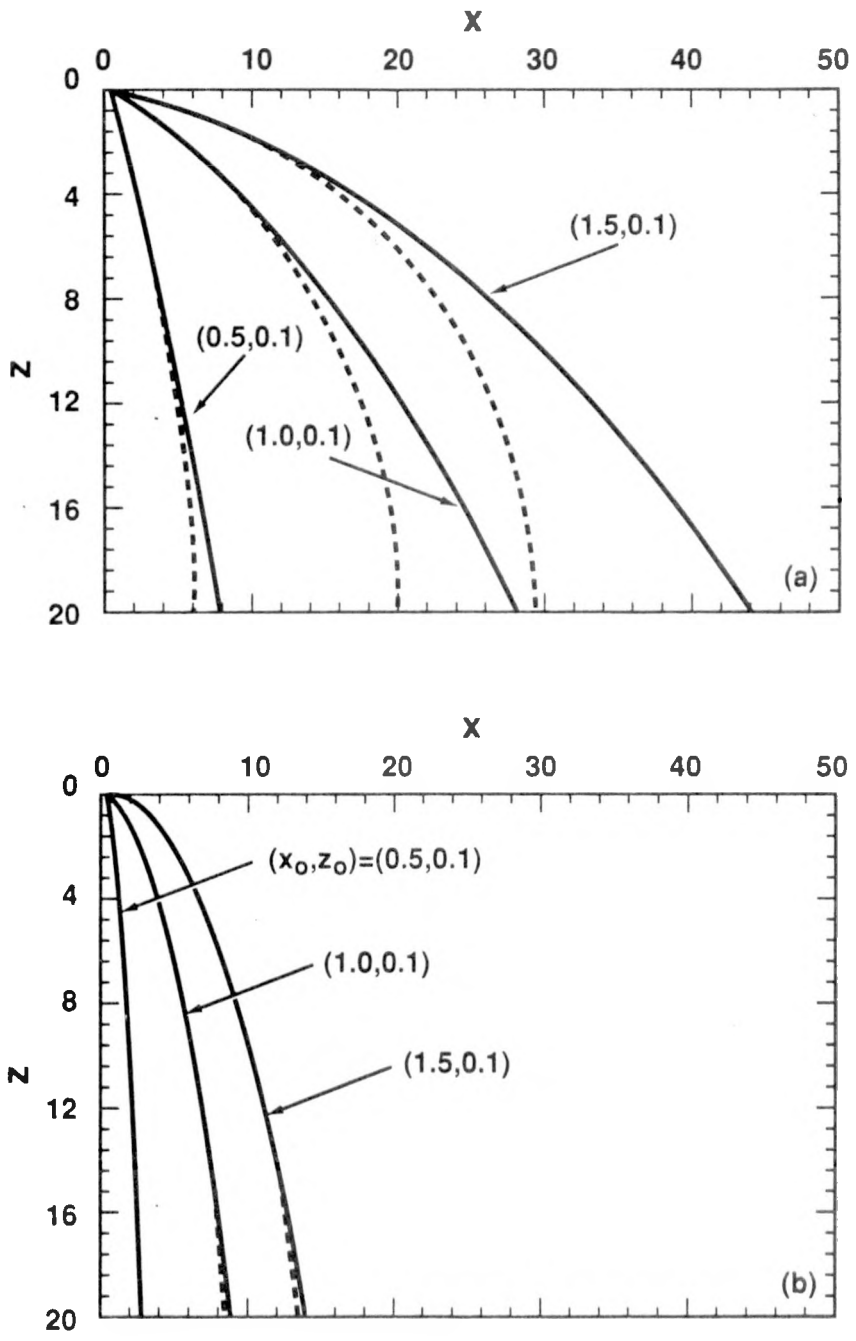

Figure 6.5. Pathlines for particles introduced at the source for (a) $a = 16^{-1}$, and (b) $a = 1$; —— $d = \infty$; $\cdots$ $d = 20$. The initial particle coordinates for the pathlines shown are (x_o, z_o) = (0.5,0.1), (1.0,0.1), and (1.5,0.1), from left to right.

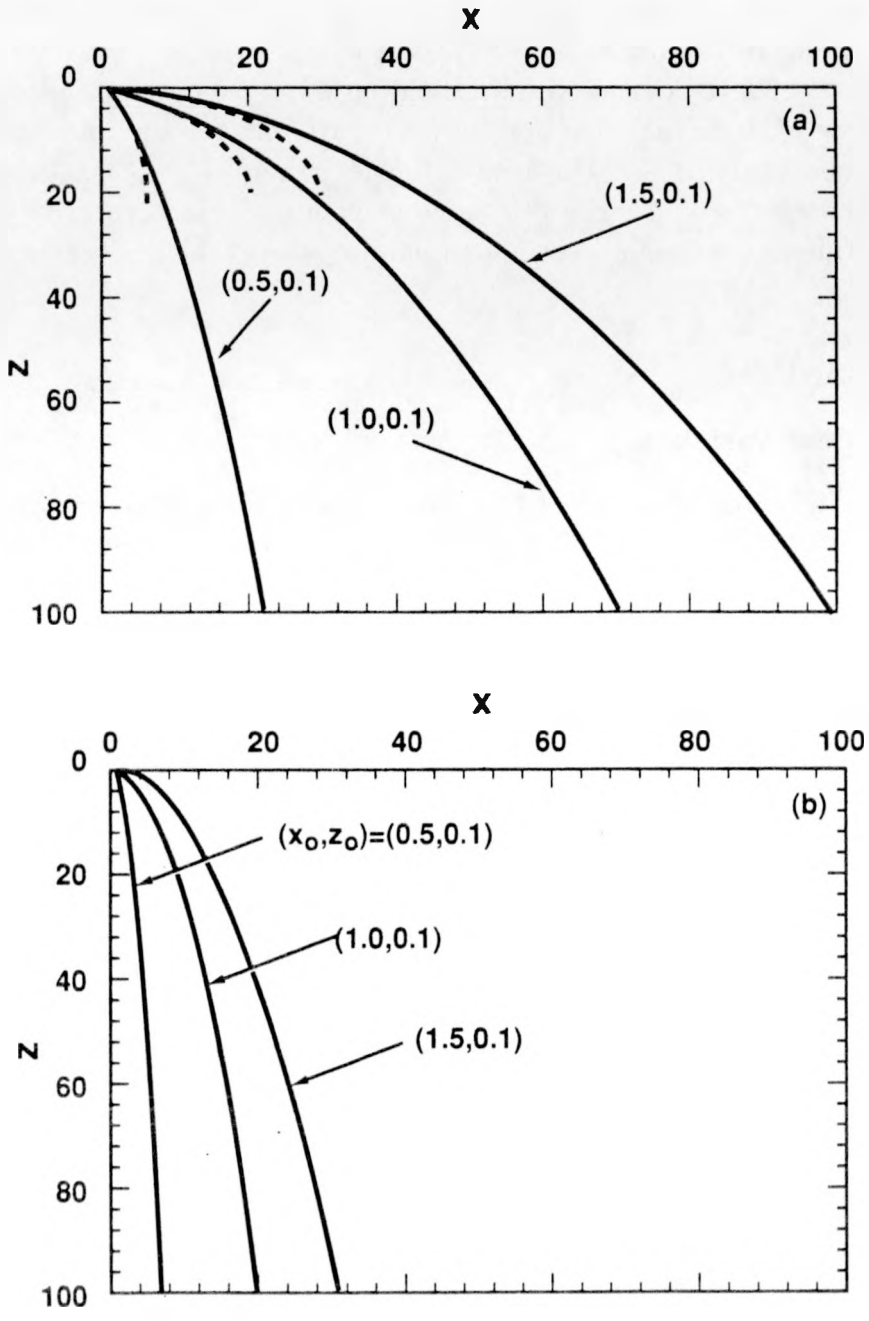

Figure 6.6. Pathlines for particles introduced at the source for (a) $a = 16^{-1}$, and (b) $a = 1$; —— $d = \infty$; $\cdots$ $d = 20$. The initial particle coordinates for the pathlines shown are (x_o, z_o) = (0.5,0.1), (1.0,0.1), and (1.5,0.1), from left to right.

substantially influences the pathlines for $ad = 20/16$ (Figure 6.5a), while the pathlines are virtually unaffected for $ad = 20$ (Figure 6.5b). A plot for $a = 16$ is not shown because, for $d = 20$, the deviation from the deep water table results is indistinguishable. In the case $a = 16^{-1}$, the deviation between pathlines for the finite and semi-infinite water tables begins for $z > 2$. For fixed d, the deviation vanishes as a increases, as shown in Figure 6.5 when $a = 1$. For this value of nondimensional sorptivity, the deviation between pathlines for the finite and semi-infinite water tables is barely discernible near $z = d$.

6.2 Specified Flux

Dimensionless Variables

When the source is described by specifying a uniform infiltration rate through the strip, we use (2.4) in place of (2.2), and the remaining boundary conditions are unchanged. We nondimensionalize the potential according to (6.1) as above with the result that on the strip

$$-\frac{\partial p}{\partial z} + ap = \frac{q_o a}{K_s}, \quad |x| < 1, \quad z = 0, \tag{6.9}$$

with the remaining boundary conditions unchanged from above, viz. (5.5) on the remainder of the surface and (6.3). The potential satisfies (5.2) and the nondimensional flux is defined by (5.3), with K_s replacing K_o. The potential is again decomposed into the capillary fringe solution, given by (6.5), and a disturbance potential defined by (6.4). The disturbance potential satisfies the same field equation and flux definition as p above, and is subject to

$$-\frac{\partial p'}{\partial z} + ap' = \frac{q_o a}{K_s} \equiv u_o', \quad |x| < 1, \quad z = 0, \tag{6.10}$$

on the source and (6.7) and (6.8) on the remainder of the domain boundaries. In the solutions to follow, only the case $u_o' = a$ $(q_o/K_s = 1)$ is considered. Because the disturbance potential satisfies homogeneous conditions otherwise, the solution for arbitrary q_o/K_s can be obtained from the solutions presented by simply rescaling p' appropriately.* The solution, $h(x, z)$, for arbitrary q_o, and hence arbitrary u_o', can be determined from the results below by defining, for example,

$$h = \frac{u_o'}{a} p', \qquad \mathbf{v} = \frac{u_o'}{a} \mathbf{u}', \tag{6.11}$$

where p' and $\mathbf{u}'$ represent the solution obtained for $q_o = K_s$. Unfolding the dimensionless variables according to their definitions, the corresponding pressure head is given by

$$\alpha\psi = \ln\left(\frac{q_o}{K_s} p' + e^{a(z-d)}\right)$$

for general q_o, in terms of p' which satisfies $q_o = K_s$ rather than (6.10). Incidentally, note that because $p'(x, d) = 0$, $\psi \sim Z - D$ for $(D - Z) = o(\alpha^{-1})$.

*There is, however, a maximum value of q_o allowable, because in the present analysis $\psi \leq 0$ everywhere. This is discussed in the following.

Results and Discussion

Once again, in analogy with the deep water table, the distribution of potential bears a relation to a and d very similar to that found for the source described by specifying the moisture. In fact, for given a and d, a contour plot of potential can be made to match reasonably well with that obtained for the Dirichlet source by adjusting q_o. There is, however, a maximum value of q_o such that the pressure head satisfies $\psi \leq 0$ everywhere. Given the linear dependence of the solution on q_o, the unique upper bound, q_o^*, for which the material is at most just saturated everywhere can be determined from the solutions for $q_o = K_s$. The maximum value of potential, p^*, is given by $p(0,0)$ and $p(0,0) = p'(0,0) + \exp(-ad)$. Hence, owing to the linearity of the problem with respect to the applied flux (as expressed in (6.11)), the upper bound q_o^* is given by (5.15), where p^* is $p(0,0)$ when $q_o/K_s = 1$, as in the present problem.

The dependence of q_o^* on a and d is shown in Figure 6.7. The results from Table 5.2 are included as the curve labelled $d = \infty$. As we noted previously for the deep water table, $q_o \to K_s$ for large a, and Figure 6.7 shows this to persist independently of d for sufficiently large a. Thus, when gravity dominates, the maximum steady infiltration rate the material is able to absorb and yet remain unsaturated beneath the source is about K_s. However, when a is small and the water table is deep, the material is able to absorb many times the saturated conductivity since the moisture is strongly absorbed laterally as well as vertically. In a nondimensional sense, as $a \to 0$, the source area takes on the form of a point source, of nondimensional strength $2aq_o/K_s$, on the scale $|\mathbf{X}| = O(\alpha^{-1})$. When d is finite, however, there is a value of ad ($ad \approx 4$) for which the maximum infiltration rate is decreased owing to the finite depth to the water table, i.e., at some ad, the capillary fringe is manifest on the surface. Indeed, for $a \to 0$, $q_o^* \to K_s$ for all finite d, since the capillary fringe holds moisture well above the water table, in fact to the height of the surface. In consequence, the porous layer is uniformly 'wet', to the degree that the material is able to transport only the rate produced by a unit head gradient, i.e., the gravitational component, K_s. Between these limits, $q_o^*(a)$ has a maximum for fixed d. When d is relatively small (e.g., $d = 1$ in Figure 6.7), the porous layer is also relatively wet throughout, owing to the proximity of the water table. The maximum in q_o^* still persists here, although it is barely discernible in the figure.

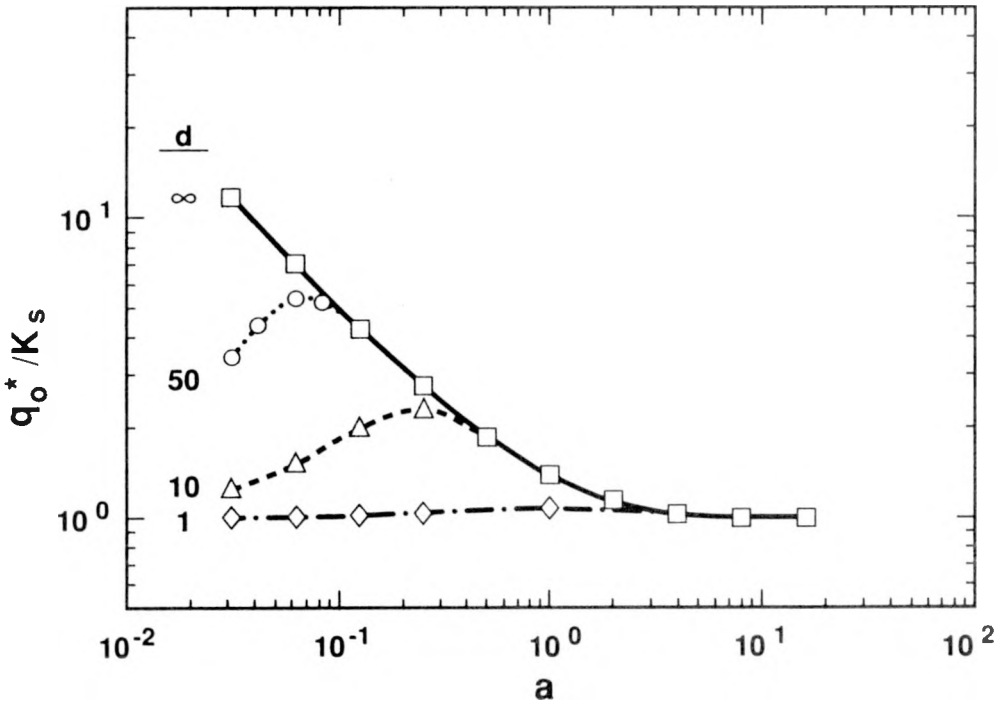

Figure 6.7. Variation of the maximum infiltration rate for unsaturated flow with dimensionless sorptivity, $a = \alpha L$, and dimensionless depth to the water table, $d = \alpha D$.

7 Summary

We have analyzed the steady infiltration from a strip source, of breadth $2L$, into an unsaturated, homogeneous, porous half-plane and finite-depth layer using a boundary integral equation method. The hydraulic conductivity is assumed to vary exponentially with the capillary pressure potential; hence, the quasi-linear transformation is utilized. The source region is described by either a specified moisture potential or by a specified value of infiltration. A water table is prescribed at some depth D below the surface for the finite-depth layer. In the half-plane problem, i.e., when the water table is deep, the material is assumed to approach a relatively dry condition far from the surface.

When the water table is deep, the distribution of moisture beneath the source is characterized by a single parameter, $a = \alpha L$, which measures the length scale over which capillary forces are comparable to gravitational forces. For $a \to 0$, capillary forces are strong and the moisture diffuses uniformly resulting in more or less circular contours of capillary pressure potential. Indeed, the lateral dispersion of fluid particles introduced at the source is found to increase with decreasing a. When $a \to \infty$, gravitational forces are dominant and the wetted lobe beneath the source is in the form of a long "finger" with maximum breadth approximately equal to the width of the source. The former distribution can be expected if the material is well graded, such as loamy soil or some welded tuff, while the latter distribution will characterize poorly graded sandy material. However, for given material type (given α) the same distributions will be a consequence of the width of the strip, $2L$. For example, the wetted lobe will be "finger-like" in tuff if $L \gg \alpha^{-1}$. This dependence of the moisture distribution on αL is qualitatively similar to that found by Wooding (1968) for the axisymmetric pond, differing mainly in the quantitive distribution of moisture.

The limit $a \to \infty$ has a heat equation analog with an analytical solution which compares very well with the full numerical solution. Furthermore, the average flux into the material over the source region is given accurately for the Dirichlet source by a simple relation determined by Weir (1986), showing that the flux is proportional to a. The numerical solutions show the relation to be accurate for $a > 1$ and that the average flux through the source approaches K_s, the saturated conductivity, for $a \gg 1$. When $a \ll 1$, the average flux is many times K_s because the moisture is strongly absorbed laterally as well as vertically.

When the source is described by a specified flux, q_o, the problem can again be parameterized solely in terms of a for the half-plane problem. The dependence of the moisture distribution on a is similar to the previous problem where the moisture is specified on the strip. Furthermore, there is a unique upper bound on the flux for which the material beneath the source remains unsaturated. Values of this critical flux, q_o^*, are determined as a function of a. These values are of interest in specifying the optimal irrigation flux for a strip source to keep the underlying porous material unsaturated, or in specifying the minimum flux to begin to saturate the material. Our results compare

satisfactorily with the two solutions given by Batu (1978) for $a = 0.2$ and 0.5. No discussion of the critical flux was offered by Batu.

The shallow water table introduces the nondimensional depth $d = D/L$, and ad as additional parameters. The characteristic nondimensional capillary fringe thickness above the water table is $ad = \alpha D$. The average infiltration, when the source is described by specifying the moisture, departs from the results for a deep water table when ad is less than about 4. The infiltration decreases with decreasing ad, compared with the maximum infiltration achieved when $d \to \infty$ and a is finite. When the source is described by specifying the infiltration rate, the maximum average infiltration allowable (q_o^*) such that $\psi < 0$ everywhere decreases from values attained for $d \to \infty$ when d is finite. However, $q_o^* \to K_s$ for large a, independent of d. Also, as $a \to 0$, q_o^* again approaches K_s for all finite d, because in this case the porous layer is uniformly wet to the extent that the material is able to only transport moisture by gravity. This is in contrast to the case $d \to \infty$, where q_o^* continually increases with decreasing a. There are no solutions for $a = 0$ and $d \to \infty$, however.

8 References

Batu, V., 1978, "Steady Infiltration from Single and Periodic Strip Sources," *Soil Sci. Soc. Am. J.*, **42**, pp. 544-549. (NNA.900711.0067)

Batu, V., and Gardner, W. R., 1978, "Steady-state Solute Convection in Two Dimensions with Nonuniform Infiltration," *Soil Sci. Soc. Am. J.*, **42**, pp. 18-22. (NNA.900711.0069)

Batu, V., 1980, "Flow Net for Unsaturated Infiltration from Periodic Strip Sources," *Water Resources Research*, **16**(2), pp. 284-288. (NNA.900711.0068)

Brebbia, C. A., 1978, *The Boundary Element Method for Engineers*, John Wiley and Sons, New York, pp. 1-5. (NNA.900919.0193)

Carey, G. F., 1982, "Derivative Calculation From Finite Element Solutions," *Computer Methods in Applied Mechanics and Engineering*, **35**, pp. 1-14. (NNA.900711.0073)

Carslaw, H. S., and J. C. Jaeger, 1973, *Conduction of Heat in Solids*, 2nd. Ed., Oxford University Press, Oxford, p. 267. (NNA.900917.0143)

Churchill, R. V., J. W. Brown, and R. F. Verhey, 1976, *Complex Variables and Applications*, 3rd. Ed., McGraw–Hill, New York, p. 317. (NNA.900727.0305)

Cruse, T. A., 1969, "Numerical Solutions in Three-Dimensional Elastostatics," *Int. J. Solids. Struct.*, **5**, pp. 1259-1274. (NNA.900403.0022)

Ingham, D. B., and M. A. Kelmanson, 1984, "Boundary Integral Equation Analyses of Singular, Potential, and Biharmonic Problems," in *Lecture Notes in Engineering*, **7**, Springer-Verlag, New York. (NNA.900522.0258)

Jaswon, M. A., and Symm, G. T., 1977, *Integral Methods in Potential Theory and Elastostatics*, Academic Press, New York. (NNA.900522.0257)

Lamb, H., 1945, *Hydrodynamics*, Dover Publications, New York, 6th Ed. (NNA.900720.0083)

Liggett, J. A., and Liu, P. L., 1983, *The Boundary Integral Equation Method for Porous Media Flow*, Allen and Unwin, London, pp. 17-33, 63-85. (NNA.901130.0016)

Martinez, M. J., and K. S. Udell, 1989, "Boundary Integral Analysis of the Creeping Flow of Long Bubbles in Capillaries," ASME: *J. Appl. Mech.*, **56**, pp. 211-217. (NNA.900403.0011)

Philip, J. R., 1968 "Steady Infiltration from Buried Point Sources and Spherical Cavities," *Water Resources Res.*, **4**(5), pp. 1039-1047. (NNA.900131.0230)

Philip, J. R., 1969, "Theory of Infiltration," *Adv. Hydrosci.*, **5**, pp. 215-296. (NNA.900122.0014)

Philip, J. R., 1984a, "Steady Infiltration from Spherical Cavities," *Soil Sci. Soc. Am. J.*, **48**, pp.724-729. (NNA.900403.0004)

Philip, J. R., 1984b, "Aspects of Quasilinear Infiltration from Surface Sources, Especially the Case $\alpha = 0$," *Water Resources Research*, **20**(5), pp. 633-635. (NNA.900711.0070)

Philip, J. R., 1989a, "The Scattering Analog for Infiltration in Porous Media," *Reviews of Geophysics*, **27**, pp. 431-448. (NNA.900711.0066)

Philip, J. R., 1989b, "Multidimensional Steady Infiltration to a Water Table," *Water Resources Res.*, **25**(1), pp. 109-116. (NNA.900403.0010)

Philip, J. R., Knight, J. H., and Waechter, R. T., 1989, "Unsaturated Seepage and Subterranean Holes: Conspectus, and the Exclusion Problem for Circular Cylindrical Cavities," *Water Resources Res.*, **25**, pp. 16-28. (NNA.900403.0006)

Philip, J. R., Knight, J. H., and Waechter, R. T., 1989, "The Seepage Exclusion Problem for Parabolic and Paraboloidal Cavities," *Water Resources Res.*, **25**, pp. 605-618. (NNA.900403.0007)

Pullan, A. J., 1990, "The Quasilinear Approximation for Unsaturated Porous Media Flow," *Water Resources Res.*, **26**, pp. 1219-1234. (NNA.901127.0188)

Pullan, A. J., and I. F. Collins, 1987, "Two- and Three-Dimensional Steady Quasi-Linear Infiltration From Buried and Surface Sources Using Boundary Element Techniques," *Water Resources Res.*, **23**, p. 1633-1644. (NNA.900403.0009)

Raats, P. A. C., 1970, "Steady Infiltration from Line Sources and Furrows," *Soil Sci. Soc. Am. Proc.*, **34**(5), pp. 709-714. (NNA.900720.0039)

Waechter, R. T., and Philip, J. R., 1985, "Steady Two- and Three-Dimensional Flows in Unsaturated Soil: The Scattering Analog," *Water Resources Res.*, **21**, pp. 1875-1887. (NNA.900403.0005)

Weir, G. J., 1986, "Steady Infiltration from Large Shallow Ponds", *Water Resources Res.*, **22**, pp. 1462-1468. (NNA.900403.0008)

Wooding, R. A., 1968, "Steady Infiltration from a Shallow Circular Pond," *Water Resources Res.*, **4**, pp. 1259-1273. (NNA.900131.0253)

Yan, Y., and I. H. Sloan, 1989, "Mesh Grading for Integral Equations of the First Kind with Logarithmic Kernel," *SIAM J. Numer. Anal.*, **26**, No. 3, pp. 574-587. (NNA.900403.0283)

Yeh, G. T., 1981, "On the Computation of Darcian Velocity and Mass Balance in the Finite Element Modeling of Groundwater Flow," *Water Resources Research*, **17**(5), pp. 1529-1534. (NNA.900711.0072)

Zachmann, D. W., 1978, "A Mathematical Treatment of Infiltration from a Line Source into an Inclined Porous Medium," *Soil Sci. Soc. Am. J.*, **42**, pp. 685-688. (NNA.900711.0071)

Appendix A. Information from, and Candidate Information for, the Site and Engineering Property Data Base and the Reference Information Base

This report contains no information from the Reference Information Base and contains no candidate information for the Reference Information Base.

This report contains no candidate information for the Site and Engineering Properties Data Base.

DISTRIBUTION LIST

1 John W. Bartlett, Director (RW-1)
Office of Civilian Radioactive
Waste Management
U.S. Department of Energy
Forrestal Bldg.
Washington, D.C. 20585

1 F. G. Peters, Deputy Director (RW-2)
Office of Civilian Radioactive
Waste Management
U.S. Department of Energy
Forrestal Bldg.
Washington, D.C. 20585

1 Ralph Stein (RW-30)
Office of Civilian Radioactive
Waste Management
U.S. Department of Energy
Forrestal Bldg.
Washington, D.C. 20585

1 M. W. Frei (RW-22)
Office of Civilian Radioactive
Waste Management
U.S. Department of Energy
Forrestal Bldg.
Washington, D.C. 20585

1 B. G. Gale (RW-23)
Office of Civilian Radioactive
Waste Management
U.S. Department of Energy
Forrestal Bldg.
Washington, D.C. 20585

1 J. D. Saltzman (RW-5)
Office of External Relations
Office of Civilian Radioactive
Waste Management
U.S. Department of Energy
Forrestal Bldg.
Washington, D.C. 20585

1 S. J. Brocoum (RW-20)
Office of Civilian Radioactive
Waste Management
U.S. Department of Energy
Forrestal Building
Washington, D.C. 20585

1 T. H. Isaacs (RW-4)
Office of Stratigic Planning
and International Programs
Office of Civilian Radioactive
Waste Management
U.S. Department of Energy
Forrestal Bldg.
Washington, D.C. 20585

1 D. H. Alexander (RW-332)
Office of Civilian Radioactive
Waste Management
U.S. Department of Energy
Forrestal Bldg.
Washington, D.C. 20585

1 J. C. Bresee (RW-10)
Office of Civilian Radioactive
Waste Management
U.S. Department of Energy
Forrestal Bldg.
Washington, D.C. 20585

1 Samuel Rousso (RW-10)
Office of Program and Resources
Management
Office of Civilian Radioactive
Waste Management
U.S. Department of Energy
Forrestal Bldg.
Washington, D.C. 20585

1 Gerald Parker (RW-30)
Office of Civilian Radioactive
Waste Management
U.S. Department of Energy
Forrestal Bldg.
Washington, D.C. 20585

1 D. G. Horton (RW-3)
Office of Quality Assurance
Office of Civilian Radioactive
Waste Management
U.S. Department of Energy
Forrestal Bldg.
Washington, D.C. 20585

1 D. E. Shelor (RW-30)
Office of Systems and Compliance
Office of Civilian Radioactive
Waste Management
U.S. Department of Energy
Forrestal Bldg.
Washington, D.C. 20585

1 L. H. Barrett (RW-40)
Office of Storage and Transportation
Office of Civilian Radioactive
Waste Management
U.S. Department of Energy
Forrestal Bldg.
Washington, D.C. 20585

1 F. G. Peters (RW-50)
Office of Contractor Business
Management
Office of Civilian Radioactive
Waste Management
U.S. Department of Energy
Forrestal Bldg.
Washington, D.C. 20585

1 Senior Project Manager for Yucca
Mountain Repository Project Branch
Division of Waste Management
U.S. Nuclear Regulatory Commission
Washington, D.C. 20555

1 NTS Section Leader
Repository Project Branch
Division of Waste Management
U.S. Nuclear Regulatory Commission
Washington, D.C. 20555

1 Repository Licensing & Quality
Assurance Project Directorate
Division of Waste Management
U.S. Nuclear Regulatory Commission
Washington, DC 20555

1 NRC Document Control Clerk
Division of Waste Management
U.S. Nuclear Regulatory Commission
Washington, D.C. 20555

1 Carl P. Gertz (RW-20)
Office of Geologic Disposal
Office of Civilian Radioactive
Waste Management
U.S. Department of Energy
Forrestal Bldg.
Washington, D.C. 20585

1 D. U. Deere, Chairman
Nuclear Waste Technical
Review Board
1100 Wilson Blvd. #910
Arlington, VA 22209-2297

1 NRC Document Control Desk
Division of Waste Management
U.S. Nuclear Regulatory Commission
Washington, D.C. 20555

5 Carl P. Gertz, Project Manager
Yucca Mountain Project Office
Nevada Operations Office
U.S. Department of Energy
Mail Stop 523
P.O. Box 98518
Las Vegas, NV 89193-8518

12 Technical Information Office
Nevada Operations Office
U. S. Department of Energy
P.O. Box 98518
Las Vegas, NV 89193-8518

1 C. L. West, Director
Office of External Affairs
Nevada Operations Office
U.S. Department of Energy
P.O. Box 98518
Las Vegas, NV 89193-8518

1 W. M. Hewitt, Program Manager
Roy F. Weston, Inc.
955 L'Enfant Plaza, Southwest
Suite 800
Washington, D.C. 20024

1 Technical Information Center
Roy F. Weston, Inc.
955 L'Enfant Plaza, Southwest
Suite 800
Washington, D.C. 20024

3 L. J. Jardine
Technical Project Officer for YMP
Lawrence Livermore National Laboratory
Mail Stop L-204
P.O. Box 808
Livermore, CA 94550

1 J. H. Nelson
Technical Project Officer for YMP
Science Applications International Corp.
101 Convention Center Dr.
Suite 407
Las Vegas, NV 89109

1 H. N. Kalia
Exploratory Shaft Test Manager
Los Alamos National Laboratory
Mail Stop 527
101 Convention Center Dr.
Suite 820
Las Vegas, NV 89109

1 Arend Meijer
Los Alamos National Laboratory
Mail Stop J514
P.O. Box 1663
Los Alamos, NM 87545

4 R. J. Herbst
Technical Project Officer for YMP
Los Alamos National Laboratory
N-5, Mail Stop J521
P.O. Box 1663
Los Alamos, NM 87545

6 L. R. Hayes
Technical Project Officer for YMP
U.S. Geological Survey
P.O. Box 25046
421 Federal Center
Denver, CO 80225

1 K. W. Causseaux
NHP Reports Chief
U.S. Geological Survey
P.O. Box 25046
421 Federal Center
Denver, CO 80225

1 R. V. Watkins, Chief
Project Planning and Management
U.S. Geological Survey
P.O. Box 25046
421 Federal Center
Denver, CO 80225

1 Center for Nuclear Waste Regulatory Analyses
6220 Culebra Road
Drawer 28510
San Antonio, TX 78284

1 D. L. Lockwood, General Manager
Raytheon Services, Inc.
Mail Stop 514
P.O. Box 93265
Las Vegas, NV 89193-3265

1 Richard L. Bullock
Technical Project Officer for YMP
Raytheon Services, Inc.
101 Convention Center Dr.
Suite P250
Las Vegas, NV 89109

1 James C. Calovini
Raytheon Services, Inc.
101 Convention Center Dr.
Suite P-280
Las Vegas, NV 89109

1 Dr. David W. Harris
YMP Technical Project Officer
Bureau of Reclamation
P.O. Box 25007 Bldg. 67
Denver Federal Center
Denver, CO 80225-0007

1 A. E. Gurrola
General Manager
Raytheon, Inc.
Mail Stop 580
P.O. Box 93838
Las Vegas, NV 89193-3838

1 M. D. Voegele
Science Applications International Corp.
101 Convention Center Dr.
Suite 407
Las Vegas, NV 89109

1 P. T. Prestholt
NRC Site Representative
1050 East Flamingo Road
Suite 319
Las Vegas, NV 89119

1 R. E. Lowder
Technical Project Officer for YMP
MAC Technical Services
Valley Bank Center
101 Convention Center Drive
Suite 1100
Las Vegas, NV 89109

1 D. L. Fraser, General Manager
Reynolds Electrical & Engineering Co.
P.O. Box 98521
Mail Stop 555
Las Vegas, NV 89193-8521

1 P. K. Fitzsimmons, Director
Health Physics & Environmental Division
Nevada Operations Office
U.S. Department of Energy
P.O. Box 98518
Las Vegas, NV 89193-8518

1 Robert F. Pritchett
Technical Project Officer for YMP
Reynolds Electrical & Engineering Co.
Mail Stop 615
P.O. Box 98521
Las Vegas, NV 89193-8521

1 D. Zesiger
U.S. Geological Survey
101 Convention Center Dr.
Suite 860 - MS509
Las Vegas, NV 89109

1 Elaine Ezra
YMP GIS Project Manager
EG&G Energy Measurements, Inc.
P.O. Box 1912
Mail Stop H-02
Las Vegas, NV 89125

2 SAIC-T&MSS Library
Science Applications International Corp.
101 Convention Center Dr.
Suite 407
Las Vegas, NV 89109

1 Dr. Martin Mifflin
Desert Research Institute
Water Resources Center
2505 Chandler Avenue
Suite 1
Las Vegas, NV 89120

1 E. P. Binnall
Field Systems Group Leader
Building 50B/4235
Lawrence Berkeley Laboratory
Berkeley, CA 94720

1 J. F. Divine
Assistant Director for Engineering Geology
U.S. Geological Survey
106 National Center
12201 Sunrise Valley Dr.
Reston, VA 22092

1 W. M. Glanzman
U.S. Geological Survey
P.O. Box 25046
Denver Federal Center
Denver, CO 80225

1 C. H. Johnson
Technical Program Manager
Nuclear Waste Project Office
State of Nevada
Evergreen Center, Suite 252
1802 North Carson Street
Carson City, NV 89710

1 T. Hay, Executive Assistant
Office of the Governor
State of Nevada
Capitol Complex
Carson City, NV 89710

3 R. R. Loux, Jr.
Executive Director
Nuclear Waste Project Office
State of Nevada
Evergreen Center, Suite 252
1802 North Carson Street
Carson City, NV 89710

1 John Fordham
Water Resources Center
Desert Research Institute
P.O. Box 60220
Reno, NV 89506

1 Prof. S. W. Dickson
Department of Geological Sciences
Mackay School of Mines
University of Nevada
Reno, NV 89557

1 J. R. Rollo
Deputy Assistant Director for
Engineering Geology
U.S. Geological Survey
106 National Center
12201 Sunrise Valley Dr.
Reston, VA 22092

1 Eric Anderson
Mountain West Research-Southwest
Inc.
2901 N. Central Ave. #1000
Phoenix, AZ 85012-2730

5 Judy Foremaster
City of Caliente
P.O. Box 158
Caliente, NV 89008

1 D. J. Bales
Science and Technology Division
Office of Scientific and Technical
Information
U.S. Department of Energy
P.O. Box 62
Oak Ridge, TN 37831

1 Carlos G. Bell, Jr.
Professor of Civil Engineering
Civil and Mechanical Engineering
Department
University of Nevada, Las Vegas
4505 South Maryland Parkway
Las Vegas, NV 89154

1 C. F. Costa, Director
Nuclear Radiation Assessment
Division
U.S. Environmental Protection
Agency
Environmental Monitoring Systems
Laboratory
P.O. Box 93478
Las Vegas, NV 89193-3478

1 J. Z. Bem
Project Manager
Bechtel National Inc.
P.O. Box 3965
San Francisco, CA 94119

1 R. Harig
Parsons Brinckerhoff Quade &
Douglas
303 Second Street
Suite 700 North
San Francisco, CA 94107-1317

1 Dr. Roger Kasperson
CENTED
Clark University
950 Main Street
Worcester, MA 01610

1 Robert E. Cummings
Engineers International, Inc.
P.O. Box 43817
Tucson, AZ 85733-3817

1 Dr. Jaak J. K. Daemen
University of Nevada
Mackay School of Mines
Reno, NV 89557-0139

1 Department of Comprehensive Planning
Clark County
225 Bridger Avenue, 7th Floor
Las Vegas, NV 89155

1 Economic Development Department
City of Las Vegas
400 East Stewart Avenue
Las Vegas, NV 89109

1 Planning Department
Nye County
P.O. Box 153
Tonopah, NV 89049

1 Director of Community Planning
City of Boulder City
P.O. Box 367
Boulder City, NV 89005

1 Commission of the European
Communities
200 Rue de la Loi
B-1049 Brussels
Belgium

1 Lincoln County Commission
Lincoln County
P.O. Box 90
Pioche, NV 89043

1 Community Planning & Development
City of North Las Vegas
P.O. Box 4086
North Las Vegas, NV 89030

1 City Manager
City of Henderson
Henderson, NV 89015

1 ONWI Library
Battelle Columbus Laboratory
Office of Nuclear Waste Isolation
505 King Avenue
Columbus, OH 43201

1 Librarian
Los Alamos Technical
Associates, Inc.
P.O. Box 410
Los Alamos, NM 87544

1 Loren Lorig
Itasca Consulting Group, Inc.
1313 5th Street SE, Suite 210
Minneapolis, MN 55414

1 James K. Lein
Department of Geography
122 Clippinger Laboratories
Ohio University
Athens, OH 45701-2979

1	6300	T. O. Hunter, Actg.
1	6310	T. E. Blejwas, Actg.
1	6310A	F. W. Bingham
1	6310	YMP CRF
1	6310	100/121441/SAND90-0252/NQ
1	6311	A. L. Stevens
1	6312	F. W. Bingham, Actg.
1	6313	L. E. Shephard, Actg.
1	6314	L. S. Costin
1	6315	F. B. Nimick, Actg.
1	6316	R. P. Sandoval
1	6317	S. Sinnock
2	6318	L. J. Erickson
1	6318	C. Crawford for Accession No. Data Base
1	6319	R. R. Richards
20	6341	WMT Library
1	6410	D. J. McCloskey, Actg.
5	3141	S. A. Landenberger
3	3151	G. L. Esch, Actg.
1	8524	J. A. Wackerly
8	3145	N. J. Pruett for DOE/OSTI
1	1510	J. C. Cummings
1	1511	D. K. Gartling
1	1511	R. R. Eaton
1	1511	P. N. Hopkins

10	1511	M. J. Martinez
10	1511	D. F. McTigue
1	1511	A. J. Russo
1	1512	A. C. Ratzel
1	1513	R. C. Dykhuizen
1	1520	L. W. Davison
1	1540	J. R. Asay
1	1550	C. W. Peterson
1	3223	P. A. Davis
1	6230	R. K. Traeger
1	6312	G. E. Barr
1	6312	P. G. Kaplan
1	6312	F. C. Lauffer
1	6313	R. W. Barnard
1	6313	M. E. Fewell
1	6313	A. H. Treadway
1	6315	R. J. Glass
1	6315	T. E. Hinkebein
1	6416	E. J. Bonano

The number in the lower right-hand corner is an accession number used for Office of Civilian Radioactive Waste Management purposes only. It should not be used when ordering this publication.

Org.	Bldg.	Name	Rec'd by	Org.	Bldg.	Name	Rec'd by